ISTANBUL TECHNICAL UNIVERSITY ★ GRADUATE SCHOOL OF SCIENCE ENGINEERING AND TECHNOLOGY

VIBRATION ANALYSIS OF A ROTATING DOUBLE TAPERED EULER-BERNOULLI BEAM FEATURING BENDING–BENDING-TORSION COUPLED USING FINITE ELEMENT METHOD

M.Sc. THESIS

Yunus Emre COŞKUN

Department of Aeronautics and Astronautics

Aeronautical and Astronautical Engineering Programme

SEPTEMBER 2019

ISTANBUL TECHNICAL UNIVERSITY ★ GRADUATE SCHOOL OF SCIENCE ENGINEERING AND TECHNOLOGY

VIBRATION ANALYSIS OF A ROTATING DOUBLE TAPERED EULER-BERNOULLI BEAM FEATURING BENDING–BENDING-TORSION COUPLED USING FINITE ELEMENT METHOD

M.Sc. THESIS

Yunus Emre Coşkun
(511151133)

Department of Aeronautics and Astronautics

Aeronautical and Astronautical Engineering Programme

Thesis Advisor: Assist. Prof. Dr. Özge Özdemir

SEPTEMBER 2019

ISTANBUL TEKNİK ÜNİVERSİTESİ ★ FEN BİLİMLERİ ENSTİTÜSÜ

EGİLME-EGİLME-BURULMA ETKİLEŞİME MARUZ KALAN İKİ EKSENDE DARALAN BİR EULER BERNOULLI KİRİŞİN DOĞAL FREKANSININ SONLU ELEMANLAR YÖNTEMİYLE İNCELENMESİ

YÜKSEK LİSANS TEZİ

Yunus Emre Coşkun
(511151133)

Uçak ve Uzay Mühendisliği Anabilim Dalı

Uçak ve Uzay Mühendisliği Programı

Tez Danışmanı: Dr. Ögrt. Üyesi Özge ÖZDEMİR

EYLÜL 2019

Yunus Emre Coşkun, a M.Sc. student of ITU Graduate School of Science Engineering and Technology student ID 511151133, successfully defended the thesis entitled "VIBRATION ANALYSIS OF A ROTATING DOUBLE TAPERED EULER-BERNOULLI BEAM FEATURING BENDING–BENDING-TORSION COUPLED USING FINITE ELEMENT METHOD", which he prepared after fulfilling the requirements specified in the associated legislations, before the jury whose signatures are below.

Thesis Advisor : **Assist. Prof. Dr. Özge Özdemir** ....
IstanbulTechnical University

Jury Members : **Prof. Dr. Metin Orhan KAYA** ....
Istanbul Technical University

Assoc. Prof. Baha ZAFER ....
Istanbul University

Date of Submission : 27 Sep 2019
Date of Defense : 27 Oct 2019

To my family,

FOREWORD

First and foremost, I am truly indebted to my supervisor Dr. Ögrt. Üyesi Özge Özdemir a for her inspiration, excellent guidance and unwavering confidence throughout my study, without which this thesis would not be in the present form.

Second of all, I would like to thank my family for providing unyielding support and encouragement over the years. They not only provided me with the best opportunities but also created a protected environment around to help me to succeed. The values instilled in me by my family have been a constant guiding force for me. I hope the completion of my thesis gives them some happiness and relief which they truly deserve.

I would like to say thanks to my friends and colleagues who helped me immensely during my days in the graduate school.

May 2019

Yunus Emre Coşkun

Aeronautical Engineer

TABLE OF CONTENTS

Page

ABBREVIATIONS

FEM **:** Finite Element Method

CG **:** Center of Gravity

APP **:** Appendix

DE **:** Differantial Equation

HSF **:**Hermitian Shape Functions

DTM **:** Differential Transform Method

BBT **:** Bending-Bending-Torsion

EBB **:** Euler Bernoulli Beam

SYMBOLS

A	: Cross sectional area
b_0	: Breadth of beam at the root section
c_b	: Breadth taper ratio
E	: Young's modulus
EA	: Axial rigidity of the beam
ω	: Natural frequency
EI	: Bending rigidity of the beam cross section
G	: Shear modulus
h_0	: Beam height at the root section
I_y	: Second momentof inertia at the y axis
k	: Shear correction factor
L	: Length of beam
ρ	.: Density of material
ρA	: Mass per unit length
θ	: Rotation angle due to bending
w	: flapwise bending displacement
w'	: flapwise bending slope
Ω	: constant rotational speed
$\overline{\Omega}$	: rotational speed parameter
v	: chordwise bending
v'	: chordwise bending slope

LIST OF TABLES

Page

LIST OF FIGURES

Page

VIBRATION ANALYSIS OF A ROTATING DOUBLE TAPERED EULER-BERNOULLI BEAM FEATURING BENDİNG–BENDİNG-TORSION COUPLED USING FINITE ELEMENT METHOD

SUMMARY

Beams are very common types of structural components. It is possible to classify beams based on their geometric configuration which can be as following: uniform, taper, thin and thick. If practically analyzed, the non-uniform beams provide a much better distribution of strength and mass than uniform beams and may supply with special functional requirements in aeronautics, architecture, innovative engineering, and other robotics applications. Design of such structures is important to resist dynamic forces, such as earthquakes and wind. It requires the basic knowledge of mode shapes and natural frequencies of those structures. In this research work, the equation of motion of a double tapered cantilever Euler beam is derived to find out the natural frequencies of the structure. Finite element formulation has been done by using principle of Hamilton. Natural frequencies and mode shapes are obtained for different taper ratios. The effect of taper ratio on mode shapes and natural frequencies are evaluated and compared. The variation of natural frequency at different speeds and different hub radius is shown in tables.

There are two general types of vibration: forced and free. If we consider free vibration, there are no externally applied forces during vibration, but an external force may have caused an initial displacement or velocity in the system. In this thesis carry out free vibration system. Simple EBB theory is used for the helicopter blade that is modeled as a long, thin beam. Rotating tapered BBT beam results are not available in open literature, the examined beam geometry is modeled in the following FEM programmes ABAQUS, ANSYS and validation is made by using the results calculated by ABAQUS and ANSYS. After the validation of the analytical models, finite element method is applied to these models to get the element matrices, i.e. element stiffness and mass matrices. Based on the number of elements used in the structural modeling code, all the element matrices are assembled by considering the finite element rules to obtain the global matrices. The boundary conditions (are fixed at the root and free at the end) are applied to the global matrices to get the reduced matrices and the matrix systems of equations are obtained for the structural models. Modal analysis is used to solve the matrix equations and the results that are obtained by solving these matrix equations of motion are compared with the previously validated analytical ones to check the accuracy and the correctness of finite element formulation and a good congruence between the results is observed.

EGİLME-EGİLME-BURULMA ETKİLEŞİME MARUZ KALAN İKİ EKSENDE DARALAN BİR EULER BERNOULLI KİRİŞİN DOĞAL FREKANSININ SONLU ELEMANLAR YÖNTEMİYLE İNCELENMESİ

ÖZET

Bu yüksek lisans tezinin amacı iki düzlemde daralan egilme-egilme-burulma etkileşimli, askı durumundaki bir helikopter palinin doğal frekanslarının daralma oranının değişimiyle nasıl değiştiğini, sonlu elemenlar yöntemiyle incelemektir.

Bu çalışmada; giriş bölümü, Euler kirişin yapısal formülasyonü, düzgün daralan kirişin formülasyonu ve sonlu elemanlar formülasyonu olmak üzere dört ana bölüm yer almaktadır.

Giriş bölümünde genel olarak kirişlerden bahsedilmiştir. Kirişler çok yaygın yapısal bileşen tipleridir ve geometrik konfigürasyonlarına göre düzgün veya daralan ve ince veya kalın olarak sınıflandırılabilirler. Euler-Bernoulli kiriş teorisi veya diğer adıyla sadece kiriş teorisi, düzgün izotropik bir kirişin elastikliğinin basitleştirilmiş bir ifadesidir. Bu teori ile kirişlerin yük taşıma ve çökme karakteristikleri hesaplanır. Zamanla düzlem teorisi ve sonlu elemanlar analizi gibi ilave analiz araçları geliştirilmiştir fakat, basit kiriş teorisi bilimin ihtiyaç duyduğu en önemli araç olmaya devam etmiştir.

Günümüzde, hava araçlarının kanat yada pallerinin modal analizleri yapılırken bir çok yöntem kullanılmaktadır. Bu yöntemlerden birisi, kanadın bir ucu sabit diğer ucu serbest Euler-Bernoulli kirişi olarak modellenip, dinamik özellikleri hakkında bilgi elde etmektir. Kirişlerin dinamik özellikleri, frekanslar ve mod şekilleri olarak tanımlanır. Bu özellikler, yapıların maruz kaldıkları titreşimlerin ve bu titreşimlere yapılar tarafından verilen cevapların incelenmesinde kullanılır. Titreşim cisimlerin sabit bir referans eksene veya nominal bir pozisyona göre tekrarlanan hareketi olarak ifade edilir. Titreşim karakteristlikleri mühendislik tasarımları açısından önemli bir etkiye sahip olabilir. Titreşim bazen zararlıdır ve kaçınılmalıdır özellikle uçak gövdeleri, kanat kökleri gibi yerlerde yorulmaya neden olur ve çatlaklar oluşturabilir, bazen de oldukça yararlıdır ve istenilir (müzik enstrümanlarında doğal frekansa denk getirmek için yapıyı titreterek rezonans özelliğinin kullanılmak istenmesi). İki durum için de titreşimin nasıl ölçüldüğü ve analiz edildiği mühendislik için önemlidir. Pratik olarak analiz edilirse, düzgün olmayan kirişler düzgün kirişlerden daha iyi bir kütle ve kuvvet dağılımı sağlar ve mimarlık, havacılık, robotik ve diğer yenilikçi mühendislik uygulamalarında özel fonksiyonel gereksinimleri karşılayabilir. Bahsedilen önemli mühendislik uygulamalarında kullanıldıkları için dönen ve daralan kirişlerin dinamik özellikleri, tasarım ve verim açısından çok önemlidir. Bu tür yapıların tasarımı, rüzgar ve deprem gibi dinamik kuvvetlere karşı koymak için de dikkate alınmaktadır. Bu durum da yapıların doğal frekansları ve mod şekilleri hakkında temel bilgileri gerektirir.

Dinamik inceleme kapsamında ilk olarak kiriş teorileri hakkında kısa bilgiler verilerek kiriş problemlerinde kullanılan hareket denklemlerinin çıkarımları yapılmıştır. İki

genel titreşim türü vardır: zorlanmış ve serbest. Serbest titreşimi düşünülürse, titreşim sırasında dışarıdan uygulanan hiçbir kuvvet yoktur, ancak harici bir kuvvet sistemde bir başlangıç yer değiştirmesine veya hızına neden olmuş olabilir. Bu tezdeki çalışmalar serbest titreşim olarak düşünülmektedir. Kayma gerilmelerinin etkisinin düşünülmediği, şekil değişimi öncesi ve sonrası kiriş kesitinin düzlemsel ve kiriş eksenine dik kaldığı Euler-Bernoulli kiriş teorisi ile helikopter pali modeli çalışılmıştır. Bu kirişlerin serbest titreşimi, iki farklı malzeme kullanılarak incelenmiştir. Modellenen paller için homojen ve izotrop kabulü yapılarak ilgili hesaplamalar sürdürülmüştür.

Yapının doğal frekanslarını bulmak için iki eksende daralan bir Euler- Bernouli kirişi modellenmiştir. Sonlu elemanlar formülasyonu, Hamilton’s prensibi kullanılarak elde edilmiştir. Farklı daralma oranları için doğal frekanslar ve mod şekilleri elde edilir. Daralma oranın doğal frekanslar ve mod şekilleri üzerindeki etkisi değerlendirilerek karşılaştırılmıştır. Farklı hızlarda ve daralma oranlarında doğal frekansın değişimi tablolarla gösterilmiştir.

Helikopter pali için ince uzun bir kiriş modellenmiş ve Euler-Bernoulli kiriş teorisi kullanılmıştır. Sonuçlar açık literatürde mevcut bulunmamakta, incelenen kiriş modeli ABAQUS ve ANSYS gibi ticari sonlu elemanlar programında modellenmiştir ve bu iki program tarafından hesaplanan sonuçlar kullanılarak doğrulama yapılmıştır.

Analitik modellerin doğrulaması yapıldıktan sonra, yapısal formülasyonun son bölümü olan sonlu elemanlar modellemesine başlanmıştır. İlk olarak deplasman alanları, polinomlar ile tanımlanmıştır. Deplesman alanlarındaki noktalar eğilme eğilme burulma etkileşimli, toplamda 10 serbestlik derecesine sahip olacak şekilde modellenmiştir. Tanımlanan deplasman alanları, eleman düğüm noktalarındaki deplasman ifadeleri cinsinden yazılarak şekil fonksiyonları elde edilmiştir. Bu şekil fonksiyonları, daha önce analitik kısımda elde edilen potansiyel ve kinetik enerji ifadelerinde kullanılarak sırasıyla eleman katılık ve eleman kütle matrisleri gibi eleman seviyesindeki matrislerin çıkarımı yapılmıştır. Eleman matrislerinin, sonlu elemanlar yöntemine uygun olarak toplanması ile tüm yapıya ait global matrisler elde edilmiştir.

Elde edilen global matris, yapısal modelleme kodunda kullanılan elemanların sayısına bağlı olarak, tüm elemanlar matrislerini sonlu elemanlar kuralları dikkate alınarak birleştirilmiştir. Bir ucu sabit, diğer ucu serbest olan sınır koşulları uygulanarak indirgenmiş matrisler elde edilmiş ve global matrislere uygulanmıştır. Yapısal modeller için denklem matrisleri elde edilmiştir. Düzgün, daralmayan Euler Bernoulli kiriş için s+onlu elemanlar yöntemi ile çözüm bulmak için elde edilen global matris için . Daralan kiriş formülasyonu, önceden elde edilen dönen eğilme-eğilme-burulma etkileşimli kirişin katılık ve kütle matrislerine entegre edilmiştir. Hareket denklemlerinden gelen matris denklemlerini çözmek için Matlab programı kullanılarak modal analiz yapılmıştır.

Bu tez kapsamında simetrik olmayan eğilme-eğilme-burulma etkileşimli Euler bernoulli kiriş kesiti de incelenmiştir ve daha önceki yapılan çalışmalarla karşılaştırılmıştır. Simetrik olmayan kirişlerin ilk üç doğal frekanası çok etkilemediği gözlemlenmiştir. Daha sonrasında yapılan çalışmalarda simetrik kiriş olarak tasarlanıp, sonuçlar bu tasarlanan kirişe göre elde edilmiştir. Bu matris çözülerek elde edilen sonuçların doğruluğunu kontrol etmek için önceden doğrulanmış analitik değerlerle karşılaştırma yapılmıştır ve sonuçlar arasında çok iyi bir uyum olduğu gözlemlenmiştir. Yapılan çalışmaya ek olarak Euler Bernoulli kirişine dönmeden kaynaklı etki verilmiştir ve bunun doğal frekans üzerine etkisi incelenmiştir. Dönen kiriş ve dönmeyen kiriş arasında karşılaştırma yapılmıştır. Elde edilen değerler bir tablo haline getirilip farklı değerlerde daralma oranına göre grafikler çizdirilmiştir ve yorumlanmıştır.

Sonuç olarak, dönen Euler kirişin doğal frekans üzerinde etkisi, dönmeyen kirişin daralma oranı ve simetrik olmayan kiriş kesiti etkisine göre daha fazla etkiye sahip olduğu gözlemlenmiştir. Bunun sebebi ise merkezkaç kuvvetinin hızın karesiyle artmasından kaynaklıdır. Farklı daralma oranına göre mod şekilleri çizilmiştir. Simetrik olmayan kiriş profili için YY eğilme modu dışında doğal frekansa etkisi yok denecek kadar azdır.

1. INTRODUCTION

Beams, have practical significance in engineering design, whose geometry and/or material properties diversify along the length, for instance they are used to reduce volume or weight as well as to increase stability and strength of structures. It has been used in many engineering applications, and there are many searches on transverse vibration of uniform beams can be found in the literature. However, if practically analyzed, non-uniform beams can provide a better or more appropriate mass and force distribution than uniform beams, and therefore meet specific functional requirements in architecture, aerospace, robotics and other innovative engineering applications countless work. Non-prismatic members are increasingly used in diversity as well as aesthetic, economic and other issues.

The design of such structures that will withstand dynamic forces such as wind and earthquake requires knowledge of the mode shapes of vibration and natural frequencies. The linear free vibration of the Euler Bernoulli tapered beam on a horizontal or vertical plane finds a wide range of application for the springs in electrical contacts and electromechanical devices.

Up to now, many scientists have found different methods to find the mode shapes and behavior of beams. Euler beam theory is used for tapered beam vibration analysis. Here, the free vibration analysis is a process that defines a structure with its natural characteristics, which are frequency and mode shapes. The change of the modal properties directly provides an indication of the structural state based on changes in mode patterns and the vibration frequencies.

There are many methods developed to calculate beam frequencies and mode shapes. Due to improvements in the calculation techniques and the availability of software, FEA is less demanding than traditional methods. Previous to development of the FEM, there existed an approximation technique for solving DE called the Method of Weighted Residuals (MWR). These formulations have displacements and rotations as the primary nodal variables, to ensure the continuity necessity each node has both slope and deflection as nodal variables. A cubic polynomial function is assumed since the beam element has four nodal variables. The clamped free beam that is being considered here is assumed to be homogeneous and isotropic. Beam of rectangular cross-section area with width and depth varying linearly are taken and elemental mass and stiffness matrices are being derived. The effects of taper ratio on the fundamental frequency and mode shapes are shown in with comparison for clamped-free beam via graphs and tables. After obtaining the results are compared with the available analytical solutions.

1.1 Purpose of Thesis

According to the literature review and previous sub-section, thefollowing objectives are determined for the present thesis;

- Derivating formulation of equation of motion of linearly tapered in two plane for rectangular cross-section EBB.
- Obtaining of HSF and the elemental mass and stiffness matrices for FEA.
- Vibration charecteristics of rotating tapered Euler-Bernoulli beam.
- Vibration charecteristics of non-rotating tapered Euler-Bernoulli beam.
- Examining of coupling effect on vibration charasteristic of EBB.

1.2 Literature Review

Özdemir and Kaya [1] determined the free vibration analysis of a rotating tapered EBB. The beam tapers linearly in the horizontal planes simultaneously. In this study, non-dimensional natural frequencies are found of the tapered EBB by using DTM.

Ozgumus and Kaya [2] derivated the differential equation from the Bernoulli-Euler equation for the natural frequencies of a tapered cantilever beam. The beam tapers linearly in the vertical planes and in the horizontal simultaneously. The effects of different taper ratio on the vibration frequency have been analyzed.

Mabie and Rogers [3] using the Bernoulli Euler's equations, investigated the free vibrations of the cantilever beams. Two configurations of interest are considered in their analysis: (a) linearly variable width and constant thickness and (b) linear variable thickness and constant width. Graphs are drawn for each case.

Ece et al. [4] derivated the modal analysis of isotropic beam with diffirent cross-section. The management equation is reduced to a normal differential equation in spatial coordinate for a family of cross-sectional area geometry with increase incrementally varying width. The beam modal analysis are obtained for three different boundary conditions such as clamped, simply supported and connected to the free ends by analytical method. Mode shapes and natural frequencies are calculated for different set of boundary conditions. It shows that the unformability in the section affects mode shapes and natural frequencies.

Bazoune & Khulief [5] derivated in this article, a beam element is obtained for modal analysis of a rotating tapered beam with rotating inertia and shear deformations. The finite model have involve linear tapering in horizontal and vertical planes and four degrees of freedom. This formulation allows any combination of uneven lengths as well as taper ratios. Clear expressions for the stiffness matrices and finite element mass are obtained using the consistent mass approach, taking into account the effects of centrifugal stifness. Numerical solutions are produced and the generalized eigenvalue problem is defined for variable taper ratios and a wide range of rotational speeds. The results are found first ten vibration modes for both hinged end and fixed conditions. Comparisons are made with numerical results and the exact solutions available in the literature.

Banerjee and Williams [6] used the Euler-Bernoulli theory and Bessel. Functions for obtaining clear expressions for complete static rigidity for bending, axial and torsional deformation of an axially loaded tapered beam. Procedures are provided to calculate the number of critical buckling loads of a clamped clamp member overrun by any test load, since therefore an existing algorithm can be used to find precise critical buckling loads of structures.

Raju et al. [7] derivated the vibration analysis of the beam using a simple FEM formulation. They applied to large amplitude vibrations for different conditions, that is, simply supported tapered beams which is linearly varying depth and width tapers.

Mabie and Rogers [8] presented the free vibrations of a tapered in two planes cantilever beam with (1) end support and (2) end mass by using the Bernoulli-Euler equation. The Euler beam was thinned linearly in the vertical planes and horizontal planes at the same time as the contraction ratio in the horizontal plane was equal to that in the vertical plane. The frequency, second, third, fourth and fifth harmonic can be easily obtained for various taper ratios. The table shows that the affect of the taper ratio on various harmonics. For in the latter case, a table and the resulting tables show the affect of the taper ratio and the ratio of the end mass to the beam mass on the fundamental frequency and higher harmonics. Although presented earlier, the free-ended beam condition is also included for comparison.

Gupta and Rao [9] studied a width and depth of linearly varying mass matrices and stiffness matrices of a twisted beam element. It is assumed that the twist angle changes linearly along the length of the beam. The affects of rotational inertia and shear deformation have been considered in the derivation of the elementary matrices.The first four mode shapes and natural frequencies have been found for cantilever beams of various breadth and depth taper ratios at variable angles of twist. The results were compared with those available.

Hodges [10] are investigated the stability of elastic torsion, lead-lag bending, and flap bending of uniform, untwisted, cantilever rotor blades for hovering flight condition. The equations of motion are obtained by simplifying the general, non-linear, partial differential equations of motion of a rotating cantilever blade. By using strip theory the aerodynamic forces are obtained. The accuracy of the results are type of mode shapes and sensitive to the number of element used in the analysis.

Ozgumus and Kaya [11] studied, Timoshenko beam featuring coupling between torsional and flapwise bending vibrations is performed on a rotating cantilever cantilever with rectangular cross section which changes linearly in two planes. Differential equations of motion are derivated by using Hamilton’s principle. A new and effective mathematical method called the Differential Transform Method (DTM) is used to find mode shapes and the natural frequencies of the taper beam. The effects of taper ratio, rotation speed parameter and core radius parameter are examined and given in tables and figures. Validation is completed from comparisons with studies in the open literature and convergence of natural frequencies.

CWS To [12] presented in this article that expressions for the mass and stiffness matrices of a tapered beam finite element model including rotary inertia and shear deformation. The element cross-section rotation is considered to be the sum of the displacement , shear, and transverse slope. Along the length of beam, dimesions of cross-sectional is vary linearly. In addition, the other was used to determine the aspect ratio over the eigenvalues of the thin walled taper beam structures. The affects of rotary inertia and shear deformation are to reduce the eigenvalues of the structure.

2. THEORY OF EULER BERNOULLI BEAM

The EBB theory or simply beamed theory, is a simplified expression of the elasticity of a smooth isotropic beam. With this theory the load bearing and collapse characteristics of the beams are calculated. Over time, additional analysis tools such as plane theory and finite element analysis have been developed, but simple beam theory remains the most important tool of science. Especially in civil and mechanical engineering areas.

Equation of Beam:The elasticity curve is defined for a beam that is made of long thin one-dimensional isotropic material

$$\frac{\partial^2}{\partial x^2}\left[EI\frac{\partial^2 u}{\partial x^2}\right] = w \tag{2.1}$$

This is known as the Euler-Bernoulli equation. If we consider the beam as a one-dimensional object in the x-axis direction, the u (x) curve defines the collapse in the beam. w is a function of x, u, and other variables. E is the modulus of elasticity and I is the inertia modulus. Here, u = u (x), w = w (x), and EI is constant, ie:

$$EI\,\frac{\partial^4 u}{\partial x^4} = w(x) \tag{2.2}$$

This equation defines the collapse of an even fixed beam and is one of the most basic elements used in engineering applications.The meanings of the terms are:

• u collapse of the beam.

• $\frac{\partial u}{\partial x}$ bending of beam.

• $EI\,\frac{\partial^4 u}{\partial x^4}$ bending moment of beam.

•$-\frac{\partial}{\partial x}\left[EI\frac{\partial^2 u}{\partial x^2}\right]$ shear stress in the beam.

This beam is defined as a one-dimensional object according to the assumptions made. The beam must be smooth, the distributed loads must not be in the plane and torsion should not be present. The tensile stress is defined as follows:

$$\sigma = \frac{Mc}{I} = Ec\frac{\partial^2 \boldsymbol{u}}{\partial \boldsymbol{x}^2} \tag{2.3}$$

The c is in the direction of u and indicates the distance between the force in the direction of application and the neutral axis. M is the bending moment. Considering the cross-section of the isotropic beam, the upper part of the pull-out occurs at the top and the compression stresses at the bottom, which are also the maximum stresses in the beam. If the neutral axis passing through the middle is a normal axis, the tensile and compression stress value is zero.

<u>Boundry Conditions:</u>The beam equation has a maximum of four boundary conditions calculated by taking the derivative according to x. The boundary conditions generally consist of model supports, ie loads, moments and other effects that affect their point.

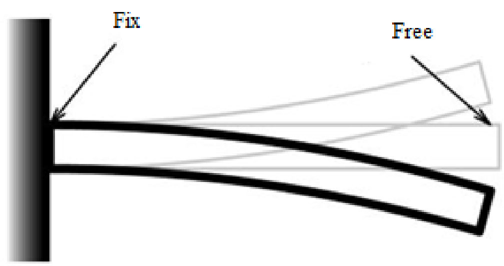

Figure 1: Cantilever Beam

An example of the support beam Figure 1: which is fixed so that it does not move at all, the other end of the beam is completely free. It is understood that when it is fixed, the bending and the collapse are zero, the bending moment and the shear force are zero. In the case where EI is constant, the left-most coordinate of x is taken as zero and the right-most side is considered to be L (the length of the L beam).

$$u\Big|_{x=0} = 0 \quad ; \quad \frac{\partial u}{\partial x}\Big|_{x=0} = 0 \ \textbf{(fixed)} \tag{2.4}$$

$$\frac{\partial^2 u}{\partial^2 x}\bigg|_{x=L} = 0 \quad ; \quad -EI\,\frac{\partial^3 u}{\partial^3 x}\bigg|_{x=L} = 0 \;\; \textbf{(free)} \tag{2.5}$$

The most common boundary conditions :

- $u = \frac{\partial u}{\partial x} = 0$ indicates that there is a fixed support.
- $u = \frac{\partial^2 u}{\partial^2 x} = 0$ indicates pin connection. (collapse and moment is zero).
- $\frac{\partial^2 u}{\partial^2 x} = \frac{\partial^3 u}{\partial^3 x} = 0$ indicates that there is no connection and therefore no load.
- $-\frac{\partial}{\partial x}\left[EI\frac{\partial^2 u}{\partial x^2}\right]$ =F indicates that there is a force F in the application point.

Load Case:The application load can be found under boundary conditions or as a function of w. Distributed load is often preferred for convenience. The boundary conditions are used in determining the loads in the model and especially in the vibration analysis.

The delta function is used as an aid when modeling point loads. For example, let's consider a beam with a fixed support L length and the F load to the top of the free end of it. Considering the boundary conditions, it can be state as follows:

$$EI\,\frac{d^4 u}{d^4 x} = 0 \tag{2.6}$$

$$u|_{x=0} = 0 \; ; \qquad \frac{\partial u}{\partial x}\bigg|_{x=0} = 0 \tag{2.7}$$

$$\frac{\partial^2 u}{\partial^2 x}\bigg|_{x=L} = 0 \qquad -EI\,\frac{\partial^3 u}{\partial^3 x}\bigg|_{x=L} = F \tag{2.8}$$

As a function,

$$EI\frac{\partial^4 u}{\partial^4 x}\bigg|_{x=L} = F\delta(x-L) \tag{2.9}$$

$$u|_{x=0} = 0 \quad ; \quad \frac{\partial u}{\partial x}\bigg|_{x=0} = 0 \tag{2.10}$$

$$\frac{\partial^2 u}{\partial^2 x}\bigg|_{x=L} = 0 \tag{2.11}$$

The boundary conditions (3. Derivative) of the shear stress were removed, otherwise there would be a contradiction here. These are the same boundary value problems and both come to the same conclusion:

$$u = \frac{F}{6EI}(3Lx^2 - x^3) \tag{2.12}$$

In applications where several point loads are loaded in different regions, u (x) has an important function. The use of this function makes the situation very simple, otherwise the beam would have to be divided into sections with 4 different boundary conditions.

Intelligent formulation with many different loads and interesting problems caused by these loads can be solved easily. For example, the vibrations in the beam can be calculated using the load as a function:

$$w(x,t) = -\mu\frac{\partial^2 u}{\partial\, t^2} \tag{2.13}$$

Here is the linear density of the μ beam and is definitely not constant. This time-dependent load change makes the equation a partial differential equation. Another interesting example is that the rotational motion of the beam is defined by the constant angular velocity:

$$w(u) = \mu\omega^2 u \tag{2.14}$$

In the Euler-Bernoulli beam theory only axial unit elongation $\mathcal{E}_{\mathbf{11}}$ is used as seen in **Figure 2** and lateral unit elongations. $\mathcal{E}_{\mathbf{12}}$ and $\mathcal{E}_{\mathbf{13}}$. are negligible.

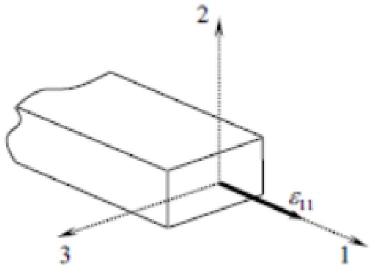

Figure 2: Unit Elongations in EBB Theory

To sum up, in this beam theory, a planar section perpendicular to the axis of the beam before displacement, after the displacement, both the plane and the vertical axis of the reference axis it is considered to still perpendicular. This feature of the Euler-Bernoulli beam is shown in Figure 3.

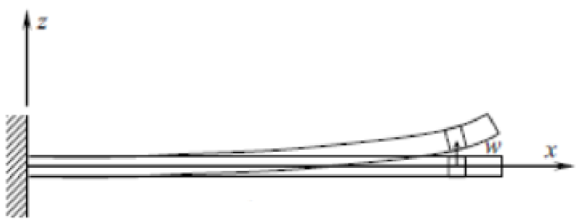

(a)

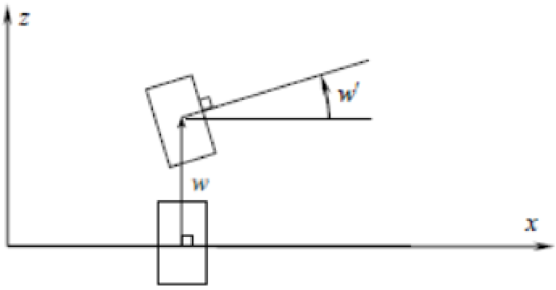

(b)

Figure 3: (a) Out-of-Plane Bending Motion of the Euler-Bernoulli Beam
(b) Out-of-Plane Bending and Shear Angle due to Bending of Beam Element

2.1 Out-of-plane bending motion of a rotating, linear Euler – Bernoulli beam

For the equation of Out-of-plane bending motion of a rotating, linear Euler – Bernoulli beam, Figure 2.8 is used for writing the necessary expressions.

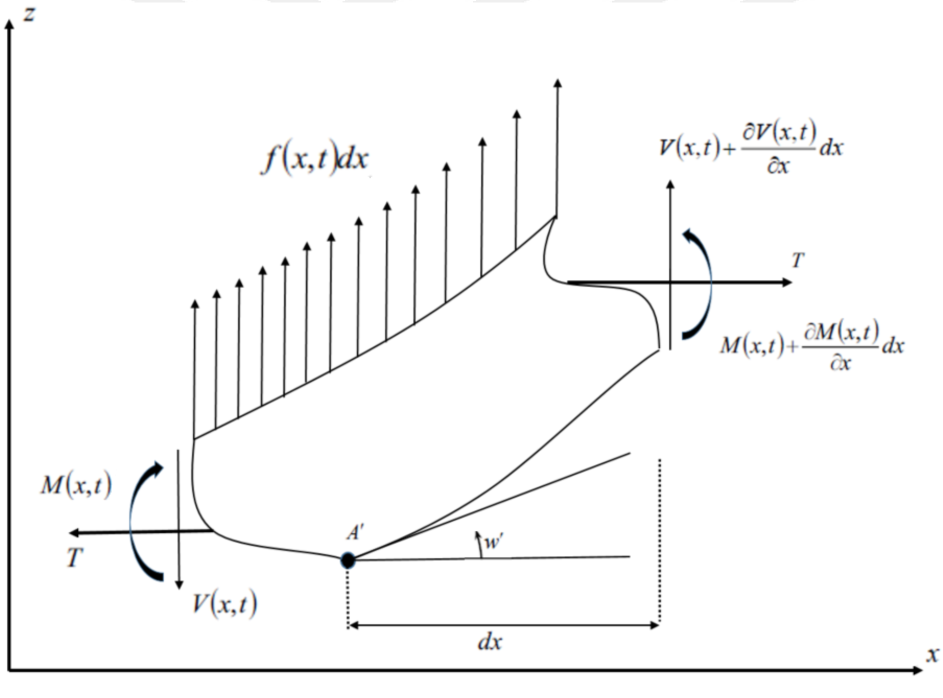

Figure 4: Forces and Moments on Euler-Bernoulli Beam Element

The connection between bending moment and beam displacement is given below.

$$M(x,t) = EI(x)\frac{\delta^2 w(x,t)}{\delta x^2} \tag{2.1.1}$$

Using forces and moments in Figure 4 and if it is written moment balance relative to A', it is accepted as counterclockwise positive direction, the following equation is obtained.

$$
\begin{aligned}
&M(x,t)+\frac{\delta M(x,t)}{\delta x}dx-M(x,t)+ \\
&\left[V(x,t)+\frac{\delta V(x,t)}{\delta x}dx\right]dx+f(x,t)dx\frac{dx}{2}-T\frac{\delta w}{\delta x}dx=0
\end{aligned}
\tag{2.1.2}
$$

After making the necessary adjustments, the equation is divided by dx and if limit $dx \to 0$ is applied, the equation (2.1.2) is reduced to the following expression.

$$
V(x,t)=T\frac{\delta w}{\delta x}-\frac{\delta M(x,t)}{\delta x} \tag{2.1.3}
$$

If the force balance is written on the vertical axis using the forces in Figure 4 and if z the direction is considered positive, the following equation is obtained.

$$
V(x,t)+\frac{\delta V(x,t)}{\delta x}dx-V(x,t)+f(x,t)dx=m(x)dx\frac{\delta^2 w(x,t)}{\delta t^2} \tag{2.1.4}
$$

After making the necessary adjustments, both sides of the equation are divided by dx and equation (2.1.4) is reduced to the following expression.

$$
\frac{\delta V(x,t)}{\delta x}+f(x,t)dx=m(x)\frac{\delta^2 w(x,t)}{\delta t^2} \tag{2.1.5}
$$

After substituting Equations (2.1.1) and (2.1.3), into the equation (2.1.5) the rotating uniform Euler-Bernoulli beam out-of-plane bending motion equation is found by Newton's approach as follows.

$$
m(x)dx\frac{\delta^2 w(x,t)}{\delta t^2}+\frac{\delta^2}{\delta x^2}\left[EI(x)\frac{\delta^2 w(x,t)}{\delta x^2}\right]-\frac{\delta}{\delta x}\left[T\frac{\delta w(x,t)}{\delta x}\right]=f(x,t) \tag{2.1.6}
$$

2.1.1 Centrifugal Force Calculation

One of the important terms in the rotating beam equations is the centrifugal force. This force is defined as the tendency of the non-flexible body rotating around any point and leaving the axis of rotation.In this section, this force expression is extracted.

A fixed free L-length beam is seen inFigure 5, from the point of rotation of the non flexiblerotor head with a radius r rotating at a constant angular ω velocity. Beam; it has the characteristic of homogeneous and isotropic material. By taking a beam element dx long over this beam and this element examined inFigure 6. The balance equations of the forces acting on this beam element are written in x direction and the centrifugal force expression is obtained.

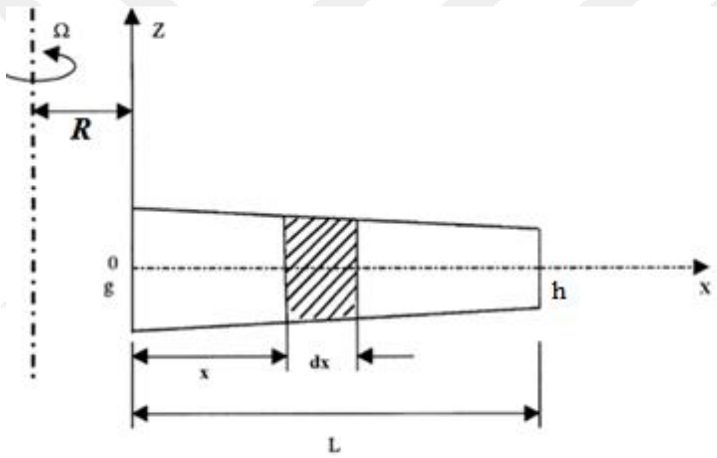

Figure 5: Rotating uniform cantilever beam model

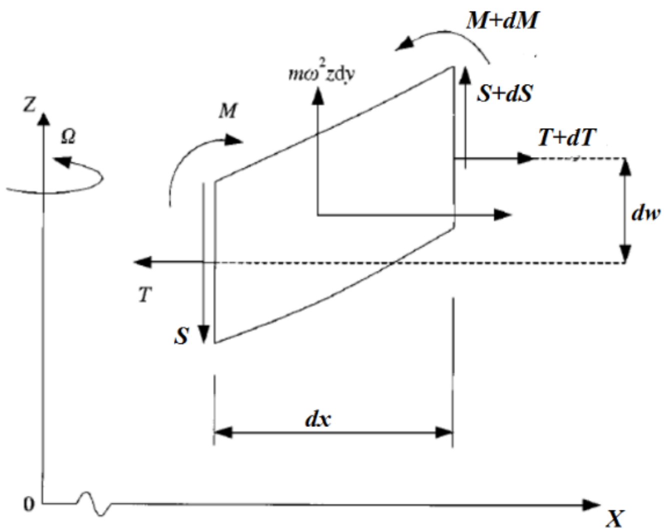

Figure 6: The forces and moments on the rotating beam element

The linear velocity of a beam element located at a distance from the rotating point $R+x$ is defined as fallow.

$$V = \Omega(R + x) \tag{2.15}$$

The centrifugal force acting on the beam element is given below.

$$F_{CF} = \frac{mV^2}{(R+x)} = m\Omega^2(R + x) \tag{2.16}$$

For the calculation of tensile force, the equilibrium equation is written in x direction.

$$T + dT - T = m\Omega^2(R + x)dx, \quad dT = m\Omega^2(R + x)dx \tag{2.17}$$

The integral of the expression in equation (2.17) is achieved by the following expression of the tensile force (centrifugal force) which acts on the entire beam and changes along the beam.

$$T = \int_0^L m\Omega^2(R + x)dx \tag{2.18}$$

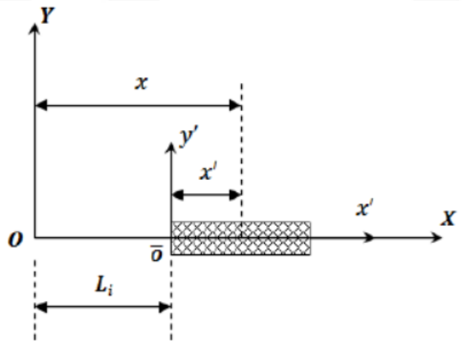

Figure 7: Rotating beam element representation for FEM

Referring to Figure 7, the centrifugal force given by Equation (2.18) can be expressed in the form of finite elements as follows

$$F_{CF}(x) = \rho A\Omega^2 \left[R(L - L_i - x') + \frac{1}{2}(L - L_i - x')(L + L_i - x')\right] \tag{2.19}$$

Where

$$L_i(i - 1)\frac{L}{n} \tag{2.20}$$

and n is the number of elements.

2.1.2 Energy expressions

The rotating Euler Bernoulli beam modeled as pre-twisted elastic blade featuring under bending-bending-torsion. Figure 8, Figure 10 are used to obtain equations of motion.

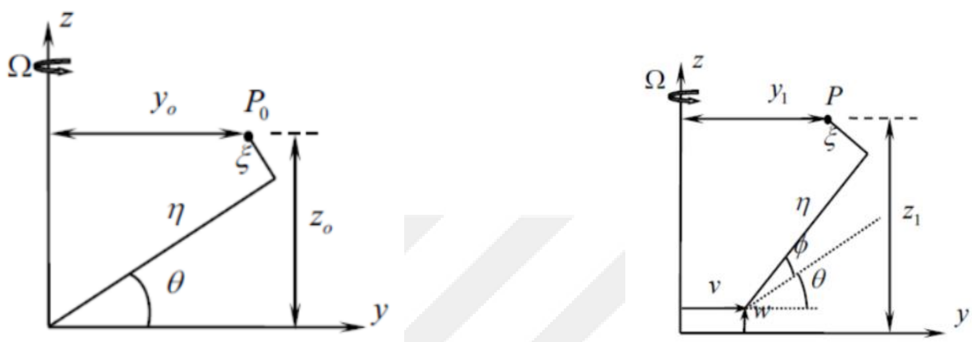

Figure 8: Section View of Rotating Euler – Bernoulli Beam with Pre-Torsion Before and After Bending-Bending-Torsional Displacements

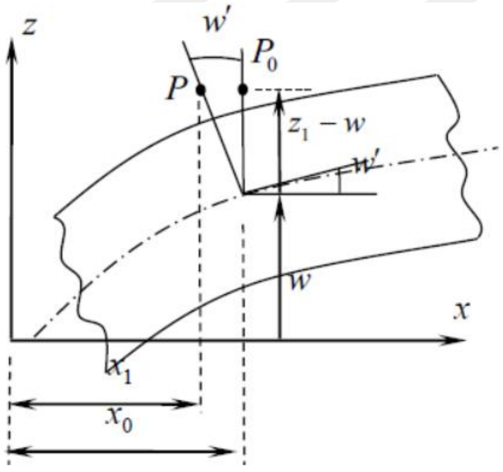
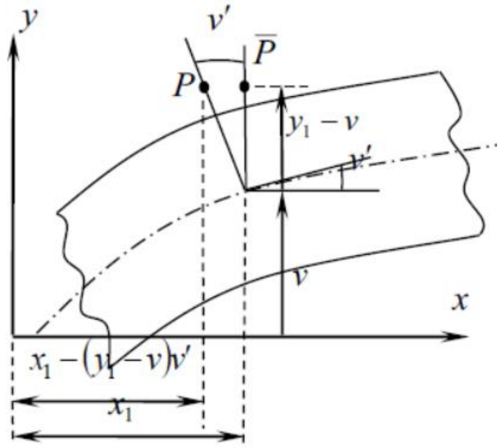

Figure 9: Top and side view

Where θ is the pretwist angle of structural undeformed beam;*w*, out-of-plane bending (flapping) displacement; *v*, chordwise bending (delay)displacement and ϕ are defined as torsional displacement.

The point referenced in Figure 8and Figure 9;P_0before displacement, P after flapwise bending displacement and P after chordwise bending displacement. The coordinates of this reference point before and after displacement are respectively as follows.

Before deformation (coordinates of P_0):

$$x_o = R + x \tag{2.21}$$

$$y_o = \eta \cos\theta - \xi \sin\theta \tag{2.22}$$

$$z_o = \eta \sin\theta + \xi \cos\theta \tag{2.23}$$

After deformation (coordinates of P):

$$x_1 = R + x + u - [\eta \sin(\theta+\phi) + \xi \cos(\theta+\phi)]w' - [\eta \cos(\theta+\phi) + \xi \sin(\theta+\phi)]v' \tag{2.24}$$

$$y_1 = v + \eta Cos(\theta+\phi) - \xi Sin(\theta+\phi) \tag{2.25}$$

$$z_1 = w + \xi Cos(\theta+\phi) + \eta Sin(\theta+\phi) \tag{2.26}$$

Here, flapwise bending and the rotation angle due to chordwise, θ, is small so it is assumed that $Sin\theta \cong \theta$. In order to research the torsional stability, the torsion angle ϕ also $Sin\phi \cong \phi$ but the second order terms are assumed that $Cos\phi \cong 1 - \frac{\phi^2}{2}$ (Hodges and Dowell, 1974). According to this assumptions Eqs. (2.24-2.26) can be derivated as below;

$$x_1 = R + x + u - \left[\eta(\phi) + \xi\left(1 - \frac{\phi^2}{2}\right)\right]w' - \left[\eta\left(1 - \frac{\phi^2}{2}\right) + \xi(\phi)\right]v' \tag{2.27}$$

$$y_1 = v + \eta\left(1 - \frac{\phi^2}{2}\right) - \xi(\phi) \tag{2.28}$$

$$z_1 = w + \xi\left(1 - \frac{\phi^2}{2}\right) + \eta(\phi) \tag{2.29}$$

Knowing that $\vec{r}_0$ and $\vec{r}_1$ are the position vectors of the reference point before and after deformation, respectively, $d\vec{r}_0$ and $d\vec{r}_1$ are given by

$$d\vec{r}_0 = (dx_0)\vec{i} + (dy_0)\vec{j} + (dz_0)\vec{k} \tag{2.30}$$

$$d\vec{r}_1 = (dx_1)\vec{i} + (dy_1)\vec{j} + (dz_1)\vec{k} \tag{2.31}$$

Here, $\vec{i}$, $\vec{j}$ and $\vec{k}$ are denotes the unit vectors in the x, y and z directions, respectively.

The components of $d\vec{r}_0$ and $d\vec{r}_1$ are expressed as follows

$$dx_0 = dx \tag{2.32}$$

$$dy_0 = d\eta \tag{2.33}$$

$$dy_1 = (v' - \eta\phi\phi' - \xi\phi')dx + \left(1 - \frac{\phi^2}{2}\right)d\eta - \phi d\xi \tag{2.36}$$

$$dz_0 = d\xi \tag{2.34}$$

$$dx_1 = \left\{1 + u' - \left[\eta(\phi) + \xi\left(1 - \frac{\phi^2}{2}\right)\right]w'' + (\xi\phi\phi' - \eta\phi')w' + (\eta\phi\phi' + \xi\phi')v' - \left[\eta\left(1 - \frac{\phi^2}{2}\right) + \xi(\phi)\right]\right\} - \left[w'(\phi) + v'\left(1 - \frac{\phi^2}{2}\right)\right]d\eta + \left[v'(\phi) - w'\left(1 - \frac{\phi^2}{2}\right)\right]d\xi \tag{2.35}$$

$$dy_1 = (v' - \eta\phi\phi' - \xi\phi')dx + \left(1 - \frac{\phi^2}{2}\right)d\eta - \phi d\xi \tag{2.36}$$

$$dz_1 = (w' - \xi\phi\phi' - \eta\phi')dx + \phi d\eta - \left(1 - \frac{\phi^2}{2}\right)d\xi \tag{2.37}$$

Here $(\ )'$ denotes differentiation with respect to the position x.

$$d\vec{r}_1 \cdot d\vec{r}_1 - d\vec{r}_0 \cdot d\vec{r}_0 = 2[\mathrm{dx}\ \ \mathrm{d}\eta\ \ \mathrm{d}\xi][\varepsilon_{\mathrm{ij}}]\begin{Bmatrix}\mathrm{dx} \\ d\eta \\ d\xi\end{Bmatrix} \tag{2.38}$$

Where $[\varepsilon_{ij}] = \begin{bmatrix}\varepsilon_{xx} & \varepsilon_{x\eta} & \varepsilon_{x\xi} \\ \varepsilon_{\eta x} & \varepsilon_{\eta\eta} & \varepsilon_{\eta\xi} \\ \varepsilon_{\xi x} & \varepsilon_{\xi\eta} & \varepsilon_{\xi\xi}\end{bmatrix}$

If Eqs. between (2.32) and (2.37) are substituted into Eq. (2.38), the components of the strain tensor $\varepsilon_{\mathrm{ij}}$ are found as follows

$$\varepsilon_{xx} = u_0' + \frac{(v')^2}{2} + \frac{(w')^2}{2} - \eta v'' - \xi w'' + \xi \phi v'' - \eta \phi w'' + \frac{1}{2}\left(\eta^2 + \xi^2\right)(\varphi')^2 \tag{2.39}$$

$$2\gamma_{x\eta} = -\xi\phi' + \eta\phi\phi' - u_0' v' + \eta v' v'' + \xi v' w'' \tag{2.40}$$

$$2\gamma_{x\xi} = \eta\phi' + \xi\phi\phi' - u_0' w' + \xi w' w'' + \eta w' v'' \tag{2.41}$$

Where , $\gamma_{x\xi}$, $\gamma_{x\eta}$ and ε_{xx} are the shear strains and the axial strain, respectively.

To find simpler expressions for strain components, see Equation. (2.39) - (2.41), if higher order terms are neglected, magnitude analysis order is performed by using scheme of ordering which is used by Hodges and Dowell (1974).

Table 1: Ordering schme for BBT coupled Euler beam formulation

Term	Order
u_0'	$O(\varepsilon^2)$
v'	$O(\varepsilon)$
w'	$O(\varepsilon)$
ϕ	$O(\varepsilon)$
ϕ'	$O(\varepsilon^2)$
v''	$O(\varepsilon^2)$
w''	$O(\varepsilon^2)$

According to the Table 1, Equation. (2.39) - (2.41) can be simplified as below

$$\varepsilon_{xx} = u_0' + \frac{(v')^2}{2} + \frac{(w')^2}{2} - \eta v'' - \xi w'' \tag{2.42}$$

$$2\gamma_{x\eta} = -\xi\phi' \tag{2.43}$$

$$2\gamma_{x\xi} = \eta\phi' \tag{2.44}$$

In the cause of the centrifugal force . the associated axial displacement u_0' and uniform strain are related to each other as follow

$$u_0' = \varepsilon_0 \frac{F_{CF}(x)}{EA} \tag{2.45}$$

where the expression of the centrifugal force. $F_{CF}(x)$. is given by

$$F_{CF}(x) = \int_x^L \rho A\Omega^2 (R+x)dx \tag{2.46}$$

The potential energy expression is given as follows

$$U = \frac{1}{2}\int_0^L \left(\iint_A E\varepsilon^2{}_{xx} + G(\gamma_{x\eta}{}^2 + \gamma_{x\xi}{}^2 d\eta d\xi \right) dx \tag{2.47}$$

The paremeter A is known as the cross-sectional area, G is the shear modulus and E is the Elasticity modulus. In Table 2, the area integrals are given.

Table 2: Area integrals for energy expressions

Area Integrals	
$\iint_A d\eta d\xi = A$	$\iint_A \eta^2 d\eta d\xi = I_z$
$\iint_A \eta d\eta d\xi = Ae$	$\iint_A \rho(\eta^2 + \xi^2) d\eta d\xi = I_\alpha$
$\iint_A (\eta^2 + \xi^2) d\eta d\xi = J$	$\iint_A \xi^2 d\eta d\xi = I_y$

The paremeter I_a is the mass moment of inertia, I_z, I_y and I_{yz} are the second moment of inertia.

$$U = \frac{1}{2}\int_0^L \left\{ F_{CF}(x) \left[(w')^2 (v')^2 \frac{I_a(\phi')^2}{\rho A} \right] + EI_z (v'')^2 + EI_y (w'')^2 + GJ(\phi')^2 \right\} dx \tag{2.48}$$

Where EI_y and EI_z are the bending rigidities and GJ is the torsional rigidity of the Euler beam cross-section.

The velocity expression has determined in order to obtain kinetic energy expression.

The velocity vector of the point P by the reason of rotation of the beam is written as follows

$$\vec{V} = \frac{\partial \vec{r}}{\partial t} + \Omega \vec{k} \times \vec{r} \tag{2.49}$$

where

$$\vec{r} = x_1 \vec{i} + y_1 \vec{j} + z_1 \vec{k} \tag{2.50}$$

If Eq.(2.50) is substituted into Eq.(2.49), the total velocity vector expression can be shown by

$$\vec{V} = (\dot{x}_1 - \Omega\, y_1)\vec{i} + (\dot{y}_1 + \Omega\, x_1)\vec{j} + \dot{z}_1 \vec{k} \tag{2.51}$$

Taking the derivatives of Eqs.(2.27)-(2.29) with respect to substituting these values into equation (2.51) and time, the velocity components are found as follows

$$\begin{aligned} V_x = {} & \dot{u}_0 + (\xi\phi\dot{\phi} - \eta\dot{\phi})w' - \left[\eta(1-\frac{\phi^2}{2}) - \xi\phi\right]\dot{v}' + (\eta\phi\dot{\phi} - \xi\dot{\phi})v' - \\ & \left[v + \eta(1-\frac{\phi^2}{2}) - \xi\phi\right]\Omega \end{aligned} \tag{2.52}$$

$$V_y = \dot{v} - (\eta\phi + \xi)\dot{\phi} + \left\{R + x + u_0 - \left[\xi(1-\frac{\phi^2}{2}) + \eta\phi\right]w' - \left[\eta(1-\frac{\phi^2}{2}) - \xi\phi\right]v'\right\}\Omega \tag{2.53}$$

$$V_z = \dot{w} + (\eta - \xi\phi)\dot{\phi} \tag{2.54}$$

This paremeter $\dot{w}$, $\dot{v}$, $\dot{\phi}$ represents derivation with in regard to time, t.

The kinetic energy equation is given by

$$\Im = \frac{1}{2}\int_0^L \left(\iint_A \rho\left(V_x{}^2 + V_y^2 + V_z^2\right) d\eta d\xi \right) dx \tag{2.55}$$

After substituting Eqs.(2.52)-(2.54) into Eq.(2.55) and with respect to the definitions given by Table 2, the following kinetic energy equation is found.

$$\Im = \frac{1}{2}\int_0^L \{\rho A\left[(\dot{v})^2 + (\dot{w})^2 + \Omega^2 (v)^2\right] + I_a (\dot{\phi})^2 -$$
$$2\rho A e_2 \left[\Omega^2 v\phi + \dot{v}\dot{\phi} - (R+x)\Omega^2 \phi v' \right] +$$
$$2\rho A e_1 \left[\dot{w}\dot{\phi} - (R+x)\Omega^2 \phi w' \right] + \tag{2.56}$$
$$2\rho I_{yz}\Omega^2 v' w' + \rho I_z \Omega^2 (v')^2 + \rho I_y \Omega^2 \left[\phi^2 + (w')^2\right]\} dx$$

Eq.(2.58) reduces to its final form is given by

$$\delta\Im = \int_0^L \{\rho A\left[(\dot{v})^2 + (\dot{w})^2 + \Omega^2 (v)^2\right] + I_a (\dot{\phi}\delta\dot{\phi}) -$$
$$2\rho A e_2 \left[\Omega^2 (v\delta\phi + \phi\delta v) + (\dot{v}\delta\dot{\phi} + \dot{\phi}\delta\dot{v}) - (R+x)\Omega^2 (\phi\delta v' + v'\delta\phi\right] +$$
$$2\rho A e_1 \left[\dot{w}\delta\dot{\phi} + \dot{\phi}\delta\dot{w} - (R+x)\Omega^2 (\phi\delta w' + w'\delta\phi) \right] + \tag{2.57}$$
$$\rho I_z \Omega^2 v'\delta v' + \rho I_{yz}\Omega^2 (v'\delta w' + w'\delta v') + \rho A(\dot{v}\delta\dot{v} + \dot{w}\delta\dot{w} + \Omega^2 v\delta v)$$
$$\rho I_z \Omega^2 (v')^2 + \rho I_y \Omega^2 \left[\phi\delta\phi + w'\delta w'\right]\} dx$$

2.1.3 Boundry Conditions and Equation of Motions

Potential and kinetic energy expressions obtained above. Hamilton's principle is applied to non-rotating, linear Euler-Bernoulli beam for obtaining equation of motion and boundary conditions. Hamilton principle as follows identified.

$$\int_{t_1}^{t_2} \delta(U - \Im - W)dt = 0 \tag{2.58}$$

The expression W denotes the virtual work of irreversible forces.

Equation of motion :

$$\rho I_z \Omega^2 v'' - \rho A\Omega^2 v + \rho I_{yz}\Omega^2 w'' + EI_z v^{iv} - (F_{CF} v')' +$$
$$2\rho A\Omega^2 e_2 \phi + \rho A\Omega^2 e_2 (R+x)\phi' + \rho A(\ddot{v} - e_2\ddot{\phi}) = 0 \tag{2.59}$$

$$\rho I_y \Omega^2 w'' + \rho I_{yz}\Omega^2 v'' + EI_y w^{iv} - (F_{CF} w')' -$$
$$\rho A\Omega^2 e_1 \phi - \rho A\Omega^2 e_1 (R+x)\phi' + \rho A(\ddot{w} - e_1\ddot{\phi}) = 0 \tag{2.60}$$

$$\frac{I_a}{\rho A}(F_{CF}\phi')' - \rho A\Omega^2\left[(R+x)(e_1 w' + e_2 v') - e_2 v\right] - GJ\phi'' + \rho I_y \Omega^2 \phi + \rho A(e_1 \ddot{w} - e_2 \ddot{v}) + I_a \ddot{\phi} = 0 \tag{2.61}$$

Boundry conditions:

At x=0,

$$v(0,t) = w(0,t) = \phi(0,t) = v'(0,t) = w'(0,t) \tag{2.62}$$

At x=L,

$$\rho I_z \Omega^2 v' + \rho I_{yz}\Omega^2 w' + EI_z v''' - F_{CF} v' + \rho A\Omega^2 e_2 (R+x)\phi = 0 \tag{2.63}$$

$$\rho I_y \Omega^2 w' + \rho I_{yz}\Omega^2 v' + EI_y w''' - (F_{CF} w')' - \rho A\Omega^2 e_1 (R+x)\phi = 0 \tag{2.64}$$

$$\phi' = v'' = w'' = 0 \tag{2.65}$$

3. MODELING OF LINEARLY TAPERED BEAMS

3.1 Euler Bernoulli Beam Model

In this thesis, free vibration analysis and mode shapes of a rotating double tapered Euler-Bernoulli beam that undergoes chordwise bending, flapwise bending and torsion vibration are performed. Structural modeling of a rotating BBT coupled Euler-Bernoulli beam is shown Figure 10.

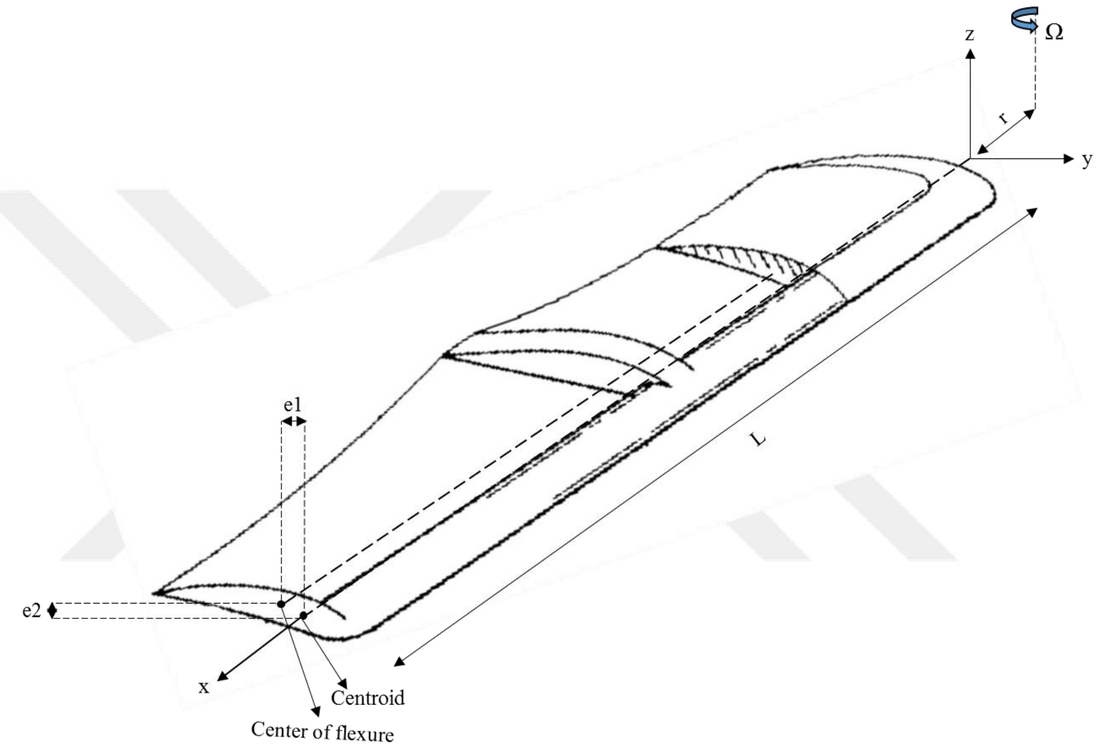

Figure 10: Helicopter blade with asymmetric cross-section.

The Euler-Bernoulli beam is assumed 10 degree of freedom, two bending, two rotation and one torsion at each node. At first the Euler beam analyzed without taper and then presented how to effect of taper ratio to vibration. Here, Euler beam of length L is shown Figure 10. The *xyz* axes is a global orthogonal coordinate system. In this thesis the Euler beam is supposed to be rotating at a constant angular velocity, Ω. The y-axis lies in the plane of rotation. The e_1 and e_2 represent the offsets of the center of flexure from the centroid in the z and y directions, in return.

The torsional vibration are not coupled with flapwise bending and chordwise bending vibrations. In addition to this, for a monosymmetric cross-section, the centroid and the shear center not coincide and the bending vibration that is in the direction of the symmetry axis is independent of the other vibrations while the bending vibration that is perpendicular to the symmetry axis is coupled with the torsional vibration (Li et al., 2004). Thus, for structures with asymmetric cross-section, bending vibrations, i.e., flapwise bending and chordwise bending, get coupled with the torsion vibration.

Differential equations of motion are obtained for a beam model that has such an asymmetric cross-section and that undergoes coupled chordwise bending-torsion, flapwise bending vibrations. The beam that is illustrated in Figure 11, is modeled as an Euler-Bernoulli beam since helicopter blades are long and thin structures.

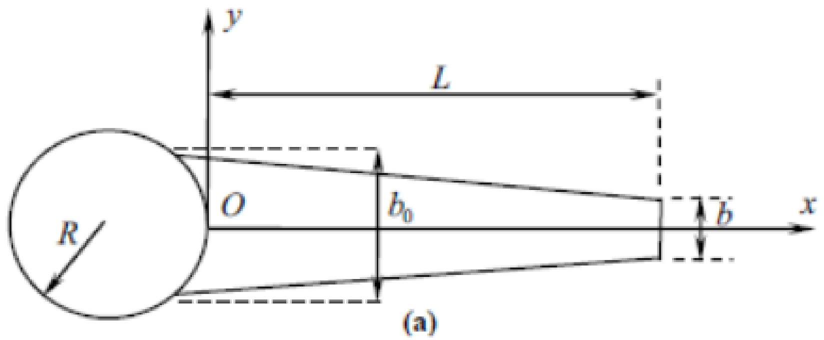

Figure 11: Euler-Bernoulli beam top view

If the main equations for the height $h(x)$, the breadth $b(x)$, the cross sectional area, $A(x)$ and the second moment of inertia, $I_y(x)$ of a Euler beam and tapers in two planes are as follows

$$b(x) = b_0\left(1 - c_b\frac{x}{L}\right)^m h(x) = h_0\left(1 - c_h\frac{x}{L}\right)^m \tag{3.1}$$

$$A(x) = A_0\left(1 - c_b\frac{x}{L}\right)^m\left(1 - c_h\frac{x}{L}\right)^m \quad \text{and} \quad I(x) = I_0\left(1 - c_b\frac{x}{L}\right)^m\left(1 - c_h\frac{x}{L}\right)^{3n} \tag{3.2}$$

where the breadth taper ratio, c_b are given by

$$c_b = 1 - \frac{b}{b_0} \text{ and } \quad c_h = 1 - \frac{h}{h_0} \tag{3.3}$$

In terms of type of taper, the values of the constants, n and m, are shown in Figure 12. This thesis analyse rectengular cross section Euler Bernoulli beam so $n = 3, m = 1$ values are used to beam that tapers linearly in two planes. Since the Elastisite modulus E, the material density, ρ and the shear modulus G are assumed to be constant, the mass per unit length ρA, the shear rigidity kAG and the flapwise bending rigidity EI_y vary according to the Eqs. (3.1) and (3.2).

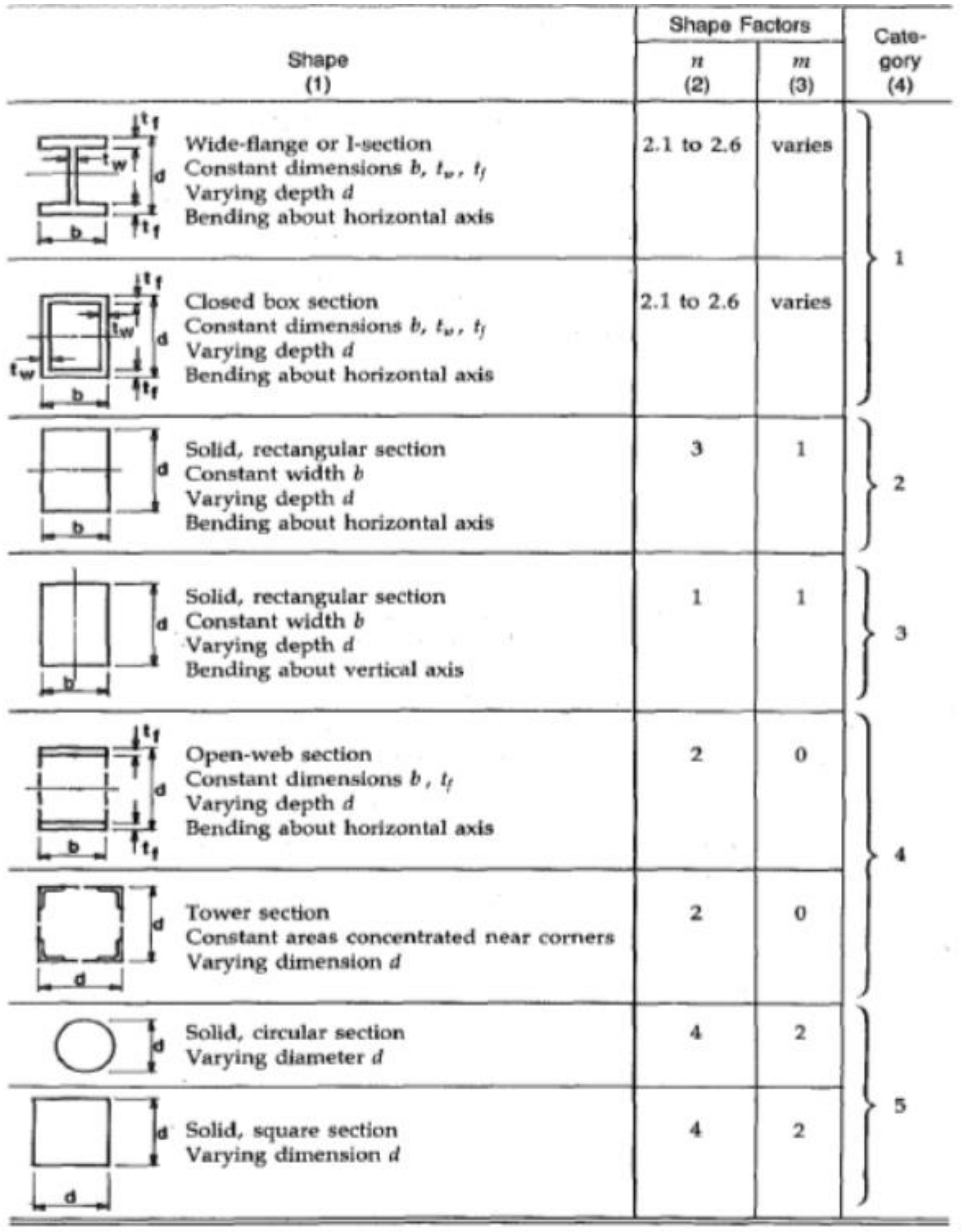

Shape (1)	Shape Factors n (2)	Shape Factors m (3)	Category (4)
Wide-flange or I-section Constant dimensions b, t_w, t_f Varying depth d Bending about horizontal axis	2.1 to 2.6	varies	1
Closed box section Constant dimensions b, t_w, t_f Varying depth d Bending about horizontal axis	2.1 to 2.6	varies	1
Solid, rectangular section Constant width b Varying depth d Bending about horizontal axis	3	1	2
Solid, rectangular section Constant width b Varying depth d Bending about vertical axis	1	1	3
Open-web section Constant dimensions b, t_f Varying depth d Bending about horizontal axis	2	0	4
Tower section Constant areas concentrated near corners Varying dimension d	2	0	4
Solid, circular section Varying diameter d	4	2	5
Solid, square section Varying dimension d	4	2	5

Figure 12: Different cross-sectional shapes of tapered beam with shape factors

3.1.1 Formulation of governing differential equation of tapered beam

A general Euler's Bernoulli beam is considered which is tapered linearly in horizontal plane. The fundamental beam vibrating equation for Bernoulli-Euler is given by

$$\frac{\partial^2}{\partial x^2}\left(EI\frac{\partial^2 y}{\partial x^2}\right)+\frac{\rho A}{g}\left(\frac{\partial^2 y}{\partial t^2}\right)=0 \tag{3.4}$$

The width is varying linearly given by

$$b=b_1+(b_0-b_1)(x/l) \tag{3.5}$$

Similarly area and moment of inertia will be varying accordingly

$$A_x\ =h[b_1+(b_0-b_1)(x/l)] \tag{3.6}$$

$$I_x=\frac{1}{12}[b_1+(b_0-b_1)(x/l)]h^3 \tag{3.7}$$

The beam area and moment of inertia at any cross-section are written after considering the variation along the length to be linear. Where ρ is the weight density, A is the area, and together 'ρA / g' is the mass per unit length, E is the modulus of elasticity and 'I' is the moment of inertia and l is the length of the beam. Here we considered only the free vibration, so considering the motion to be of form$y(x,t)=z(x)\,sin(\omega\ t)$, so applying the following relation to the fundamental beam equation we get

$$\frac{\partial^2}{\partial x^2}\left(EI\frac{\partial^2 y}{\partial x^2}\right)=\frac{\rho A}{g}(\omega^2 z) \tag{3.8}$$

Depending on the number of elements used in the developed structural modeling code, the element matrices are assembled by considering the finite element rules to obtain the global matrices. The boundary conditions of rotor blade, i.e. $w\ (0,t)$= $w'=(0,t)=\Phi\ (0,t)=0$, are applied to the global matrices to get the reduced matrix equations of motion that are given below

$$[M^s]\{\ddot{q}\}+[K^s]\{q\}=\{0\} \tag{3.9}$$

Due to rotating beam, additional terms appear in the element matrices because of the centrifugal force. These terms are derivated Eq.(2.19) by using FEM formulation for obtaining the centrifugal force.

Firstly, the modal matrix, $[\Phi]$, is calculated by using the eigenvectors obtained by solving the following determinant

$$|-\omega^2[M^s] + [K^s]| = 0 \tag{3.10}$$

The transpose of the model matrix

$$-\omega^2[I] + [\lambda^2] = \{0\} \tag{3.11}$$

Here $[\lambda^2]$ is the diagonal matrix, $[I]$ is the identity matrix of natural frequencies.

4. FINITE ELEMENT METHOD

Aircraft structures require computer analysis due to operation panels, support bars, beams and it consists of thousands of structures like frames. Computer based on specific approaches for the analysis of such structures finite element method is used.

In general, the modeling of such a structure, a small number of elements, simplified geometric details, physical the features are as accurate as possible; but without detail format. The results obtained by running this model, about the overall behavior of the structure information as compared to small hand accounts an idea of whether or not an approach data.

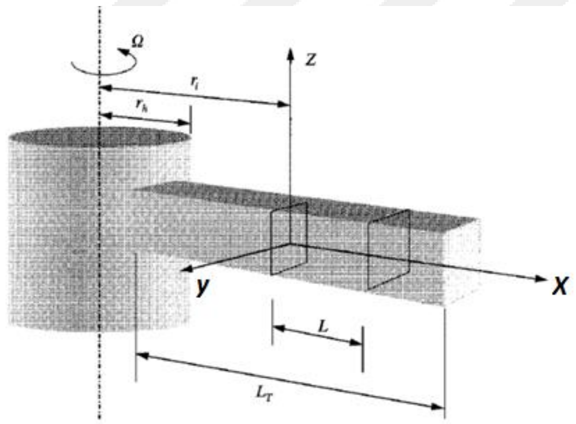

Figure 13: Rotor blade finite element model divided small elements

In addition to the analytical method, the finite element method is widely used in the solution of engineering problems. Modal analysis of a beam by using FEM, natural frequency values and mode shapes can be found. With this method, vibration problems can be solved easily. The problem is first divided into small elements in Figure 13. Providing the solution separately in these divided elements ease and accuracy.

The assemblage of such small elements represents the whole body. Each small elements are solved individually then combined to obtain solution for the whole body. With the development of computer systems, difficult vibration problems are solved more easily and in a short time. Especially analytical solution with finite element method based programs such as ANSYS, ABAQUS CAE, Nastran impossible vibration problems can be solved easily. The most used of these programs ANSYS computerized numerical analysis program, as well as stress analysis, acoustic analysis, as well as operations, natural frequency and mode shapes are easily it can be found.

4.1 Calculation of Shape Function

The main axis of the beam is discretized using straight two-noded 1D Euler beam finite elements having a uniform cross-sectional shape and mass distribution within each element.

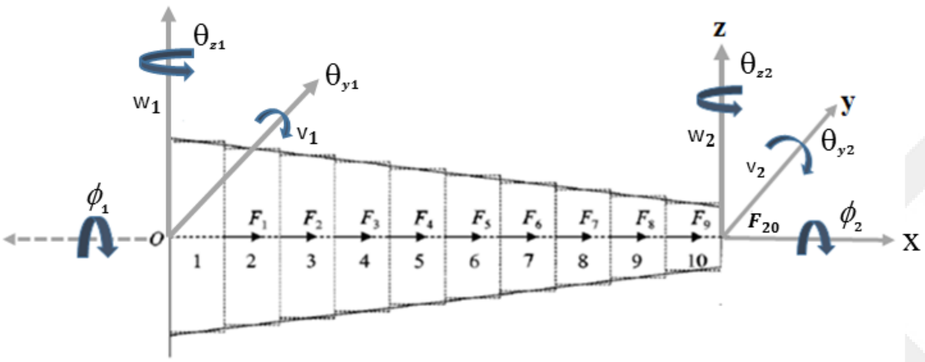

Figure 14: BBT Euler beam finite element model.

Obtaining of shape functions is fundamental task in any finite element implementation. Genalrelly two-dimensional beams are used for identical to matrix of structures and their analysis using the finite element formulation. Euler-Bernoulli beam equation assumption that the plane is normal to the neutral axis before deformationneutral axis after deformation. Because there are four nodal variables for the beamelement with a cubic polynomial function for ν(x), is assumed as

$$\nu = a_0 + a_1 x + a_2 x^2 + a_3 x^3 \tag{3.9}$$

$$w = a_4 + a_5 x + a_6 x^2 + a_7 x^3 \tag{3.10}$$

$$\theta y = v' = a_1 + a_2 x + a_3 x^2 \tag{3.11}$$

$$\theta z = w' = a_5 + a_6 x + a_7 x^2 \tag{3.12}$$

$$\Phi = a_8 + a_9 x \tag{3.13}$$

where θz is the angle due to chordwise bending , ν is the chorwise bending, w is the flapwise bending, θy is the angle due to flapwise bending, and ϕ is the torsion angle.

$$V(x)=[1 \;\; x \;\; x^{2} x^{3}]\begin{bmatrix} a_0 \\ a_1 \\ a_2 \\ a_3 \end{bmatrix} \tag{3.14}$$

$$V(x)= [C][\alpha] \tag{3.15}$$

For convenience local coordinate system is taken x_1=0, x_2=L that leads to

$$\begin{bmatrix} v_1 \\ w_1 \\ \theta_{z1} \\ \theta_{y1} \\ \phi_1 \\ v_2 \\ w_2 \\ \theta_{z2} \\ \theta_{y2} \\ \phi_2 \end{bmatrix} = \begin{bmatrix} 1 & 0 & 0 & 0 & 0 & 0 & 0 & 0 & 0 & 0 \\ 0 & 0 & 0 & 0 & 1 & 0 & 0 & 0 & 0 & 0 \\ 0 & 1 & 0 & 0 & 0 & 0 & 0 & 0 & 0 & 0 \\ 0 & 0 & 0 & 0 & 0 & 1 & 0 & 0 & 0 & 0 \\ 0 & 0 & 0 & 0 & 0 & 0 & 0 & 0 & 1 & 0 \\ 1 & L & L^2 & L^3 & 0 & 0 & 0 & 0 & 0 & 0 \\ 0 & 0 & 0 & 0 & 1 & L & L^2 & L^3 & 0 & 0 \\ 0 & 1 & 2L & 3L^2 & 0 & 0 & 0 & 0 & 0 & 0 \\ 0 & 0 & 0 & 0 & 0 & 1 & 2L & 3L^2 & 0 & 0 \\ 0 & 0 & 0 & 0 & 0 & 0 & 0 & 0 & 1 & L \end{bmatrix} \begin{bmatrix} a_0 \\ a_1 \\ a_2 \\ a_3 \\ a_4 \\ a_5 \\ a_6 \\ a_7 \\ a_8 \\ a_9 \end{bmatrix} \tag{3.16}$$

Where

$$\{b\}=[A]\{a\} \tag{3.17}$$

$$\{a\}=[A]^{-1}\{b\} \tag{3.18}$$

Eq. (3.14) can be writen as

$$V(x)=[C][A]^{-1}\{b\} \tag{3.19}$$

$$V(x)=[N]\{b\} \tag{3.20}$$

Where

$$[N]=[C][A]^{-1} \tag{3.21}$$

Matrix of shape functions are

$$[N_v]=\begin{bmatrix} 1-\dfrac{3x^2}{L^2}+\dfrac{2x^3}{L^3} & 0 & 0 & x-\dfrac{2x^2}{L}+\dfrac{x^3}{L^2} & 0 \\ \dfrac{3x^2}{L^2}-\dfrac{2x^3}{L^3} & 0 & 0 & \dfrac{-x^2}{L}+\dfrac{x^3}{L^2} & 0 \end{bmatrix}$$

$$[N_w]=\begin{bmatrix} 0 & 1-\frac{3x^2}{L^2}+\frac{2x^3}{L^3} & x-\frac{2x^2}{L}+\frac{x^3}{L^2} & 0 & 0 \\ 0 & \frac{3x^2}{L^2}-\frac{2x^3}{L^3} & \frac{-x^2}{L}+\frac{x^3}{L^2} & 0 & 0 \end{bmatrix}$$

$$[N_{\theta z}]=\begin{bmatrix} -\frac{6x}{L^2}+\frac{6x^2}{L^3} & 0 & 0 & 1-\frac{4x}{L}+\frac{3x^2}{L^2} & 0 \\ \frac{6x}{L^2}-\frac{6x^2}{L^3} & 0 & 0 & \frac{-2x}{L}+\frac{3x^2}{L^2} & 0 \end{bmatrix}$$

$$[N_{\theta y}]=\begin{bmatrix} 0 & \frac{6x}{L^2}+\frac{6x^2}{L^3} & 1-\frac{4x}{L}+\frac{3x^2}{L^2} & 0 & 0 \\ 0 & \frac{6x}{L^2}-\frac{6x^2}{L^3} & \frac{-2x}{L}+\frac{3x^2}{L^2} & 0 & 0 \end{bmatrix}$$

$$[N_{\phi}]=\begin{bmatrix} 0 & 0 & 0 & 0 & 1-\frac{x}{L} & 0 & 0 & 0 & 0 & \frac{x}{L} \end{bmatrix}$$

$[Nv]$, $[Nw]$, $[N\theta_y]$, $[N\theta_z]$, $[N\phi]$ are the shape functions of euler bernoulli beam which is undergoes bending bending torsion.

From shape function and energy derivation which is include taper equation the element stiffness and mass matrices are found as follows;

$$\begin{aligned}
[K^e]=\int_0^L \Bigg\{ & F_{cf}(x)\left(\left[\frac{dN_w}{dx}\right]^T\left[\frac{dN_w}{dx}\right]+\left[\frac{dN_v}{dx}\right]^T\left[\frac{dN_v}{dx}\right]\right)+ \\
& \frac{I_a}{\rho A_0\left(1-c_b\frac{x}{L}\right)\left(1-c_h\frac{x}{L}\right)}\left[\frac{dN_\phi}{dx}\right]^T\left[\frac{dN_\phi}{dx}\right]- \\
& EI_{z0}\left(1-c_b\frac{x}{L}\right)^3\left(1-c_h\frac{x}{L}\right)\left[\frac{d^2N_v}{dx^2}\right]^T\left[\frac{d^2N_v}{dx^2}\right]+ \\
& EI_{y0}\left(1-c_h\frac{x}{L}\right)^3\left(1-c_b\frac{x}{L}\right)\left[\frac{d^2N_w}{dx^2}\right]^T\left[\frac{d^2N_w}{dx^2}\right]+ \\
& GJ\left[\frac{dN_\phi}{dx}\right]^T\left[\frac{dN_\phi}{dx}\right]\Bigg\}dx
\end{aligned} \tag{3.22}$$

$$
\begin{aligned}
\left[M^{e}\right]=\int_{0}^{L}\Bigg\{&\rho A_{0}\left(1-c_{b}\frac{x}{L}\right)\left(1-c_{h}\frac{x}{L}\right)\left(\left[N_{w}\right]^{T}\left[N_{w}\right]+\left[N_{v}\right]^{T}\left[N_{v}\right]\right)+\\
&I_{a}\left[N_{\phi}\right]^{T}\left[N_{\phi}\right]+\\
&\rho A_{0}e_{1}\left(1-c_{b}\frac{x}{L}\right)\left(1-c_{h}\frac{x}{L}\right)\left(\left[N_{w}\right]^{T}\left[N_{\phi}\right]+\left[N_{\phi}\right]^{T}\left[N_{w}\right]\right)-\\
&\rho A_{0}e_{2}\left(1-c_{b}\frac{x}{L}\right)\left(1-c_{h}\frac{x}{L}\right)\left(\left[N_{v}\right]^{T}\left[N_{\phi}\right]+\left[N_{\phi}\right]^{T}\left[N_{v}\right]\right)\Bigg\}dx
\end{aligned}
\tag{3.23}
$$

Where $[K^e]$ is the element stiffness matrix obtained from the kinetic energy and $[M^e]$ is the element mass matrix obtained from the potential energy.

5. NUMERICAL ANALYSIS

5.1 Validation of the strucural model

Nonrotating BBT beam example is solved to validate the built structural model. Geometrical and material properties are given below in Table 3 .

Table 3: Geometrical and material properties of the nonrotating bending-bending-torsion coupled uniform beam model.

Property	Value	Property	Value
E	$213.9*10^9 N/m^2$	L	$0.1524\ m$
I_y	$34.96*10^{-12} m^4$	GJ	$9.14 m^2$
I_z	$2.7928*10^{-9} m^4$	I_a	$0.502\ kg\ m$
A	$58.97\ m^2$	ρ	$7859\ kg/m^3$
e_1	$0.1930\times10^{-3} m$	e_2	$1.1938\times10^{-3} m$

Results are compared with Rao and Carnegie (1970). Carnegie and Dawson (1971) .

Table 4: Non-rotating BBT Euler Beam frequencies (Hz)

Mode	Present		Rao and Carnegie		Carnegie and Dawson	
	Uncoupled	Coupled	Uncoupled	Coupled	Uncoupled	Coupled
1st ZZ Bending	96.7816	96.7813	96.9	96.9	96.9	96.9
2nd ZZ Bending	606.52	606.25	607	606.5	607.3	607.3
1st YY Bending	865.022	841.02	869	841.2	868.4	845.8
Torsion	1052.02	1092.37	1048.5	1072.9	1048.23	1074.02

In Table 4, the first two ZZ bending modes are not changing much by coupling effect. Although e_2 value much bigger than e_1, YY Bending mode has a significant reducing according to the results. In addition, the uncoupled mode is lower than the coupled torsion mode. As a result, although coupling has an increasing effect on the torsion modes, it has a reducing effect on the bending modes.

After validation non-rotating BBT beam, rotating Euler-Bernoulli beam is modeled and validate by using ABAQUS.

Table 5: Rotating BBT Euler Beam frequencies (Hz)

Mode	$e_1 = 0$ and $e_2 = 0$		$e_1 = 0.1930 * 10^{-3}$ and $e_2 = 0$		$e_1 = 0$ and $e_2 = 1.1938 * 10^{-3}$	
	50 rad/sn	100 rad/sn	50 rad/sn	100 rad/sn	50 rad/sn	100 rad/sn
1st ZZ Bending	97.17	98.32	97.17	98.32	97.17	98.32
2nd ZZ Bending	606.61	607.62	606.59	607.61	606.61	607.62
1st YY Bending	860.99	861.12	861	861.13	841.04	841.16
Torsion	1052.32	1052.42	1052.74	1052.84	1091.99	1092.09

The first four modes are given Table 5 and different coupling value and angular velocity has been viewed. Natural frequencies are calculated with different condition i.e. $\Omega = 50\,rad/sn,\ e_1 = 0, e_2 = 1.1938 * 10^{-3}$ and $\Omega = 100\,rad/sn,\ e_1 = 0.1930 * 10^{-3}, e_2 = 0$. By reason of the increasing centrifugal force that makes the beam stiffer, rotational speed has an increasing affect on the natural frequencies.

For numerical analysis a taper beam is considered with the following properties:

Table 6: Geometrical and material properties of the rotating bending-bending-torsion coupled uniform beam model.

Property	Value	Property	Value
E	$70*10^9$ N/m^2	L	$3\ m$
I_y	$1.172 * 10^{-5} m^4$	GJ	$1.172 * 10^{-5} m^4$
I_z	$1.45 * 10^{-9} m^4$	I_a	$0.502\ kg\ m$
b	$0.02848\ m$	ρ	$3200\ kg/m^3$
h	$0.078\ m$	e_1	$9.36 \times 10^{-3} m$
e_2	0		

Any paper that studies a rotating coupled Euler-Bernoulli beam is not present in open literature. For these reason, Euler Bernoulli beam model is built in ABAQUS and ANSYS to validate the results of the present research. The the geometrical and material properties of this beam model are presented in Table 6.

Table 7: Free natural frequencies (Hz) of nonrotating uniform Euler Bernoulli beam. Ω=0

Mode	Present	ABAQUS	ANSYS
1	6.64	6.6215	6.5458
2	23.31	23.21	23.745
3	41.55	41.172	41.107
4	116.1	116.17	115.72

In Table 7, variation of the coupled natural frequencies and the results are compared with the ones given by commercial program ABAQUS and ANSYS. Subsequent to obtaining natural frequencies of non rotating Euler bernoulli beam, rotating Euler bernoulli beam is examined. First four natural frequencies of rotating BBT Euler beam are shown in Table 8 and the results are compared with Özdemir, Phd thesis. The results are quite similar.

Table 8: Free natural frequencies with regard to rotational speed 50 (rad/sec). **Ω**=50

Mode	Present (Hz)	Özdemir, PhD Thesis (Hz)
1	10.83	10.88
2	24.04	24.87
3	46.07	46.21
4	120.6	120.87

After discretizing to 20 numbers of elements, natural frequencies of the BBT tapered beam are calculated using MATLAB program and shown in Figure 15.

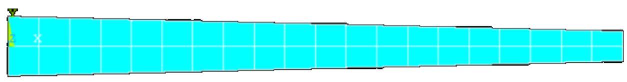

Figure 15: c_b =0.5,
$c_h = 0$, Tapered Euler Bernoulli Beam in ANSYS

Table 9: $c_b = 0.5$,
$\boldsymbol{c_h = 0}$, Natural Frequancy Tapered Euler Bernoulli Beam

Mode Number	Present MATLAB	Frequency in ANSYS (Hz)
1	8.01	8.03
2	25.33	25.84
3	43.76	43.86
4	117.51	118.5

In Figure 16, first four natural frequencies of BBT Euler Bernoulli Beam and mode shapes are shown.

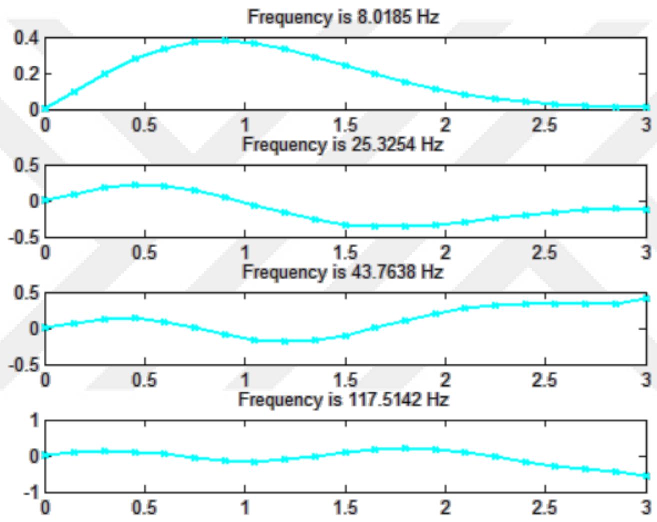

Figure 16: c_b =0.5,
$\boldsymbol{c_h = 0}$, Mode Shape of Tapered Euler Bernoulli Beam

Table 10: c_b =0.8,
$\boldsymbol{c_h = 0}$, Natural Frequancy Tapered Euler Bernoulli Beam in ANSYS

Mode Number	Present MATLAB	Frequency in ANSYS (Hz)
1	9.9	9.68
2	28.39	27.54
3	47.41	47.436
4	105.6	105.88

Table 11: $c_b = 0.5$,
$\boldsymbol{c_h = 0.5}$, Natural Frequancy Tapered Euler Bernoulli Beam in ANSYS

Mode Number	Present MATLAB	Frequency in ANSYS (Hz)
1	8.68	8.71
2	30.52	30.498
3	36.9	36.959
4	91.81	92.527

Different taper ratios are examined for BBT Euler beam in above tables. The analytical results are compared with Ansys. It is seen that there is a good agreement between the results of ANSYS and the results of the this study which proves the accuracy and correctness of the built structural model. In below tables, the variation of the natural frequencies of a tapered BBT Euler beam with respect to the variable taper ratio, Cb ,Ch and the rotational speed parameter, Ω, are shown.

Table 12: 1.Natural Frequancy of Non-rotating BBT Euler Bernolli Beam

	c_b								
c_h	0	0.1	0.2	0.3	0.4	0.5	0.6	0.7	0.8
0	6.56	6.77	7.02	7.30	7.63	8.02	8.50	9.10	9.90
0.1	6.65	6.87	7.11	7.39	7.72	8.12	8.60	9.21	10.01
0.2	6.76	6.98	7.22	7.50	7.83	8.23	8.71	9.32	10.12
0.3	6.89	7.10	7.35	7.63	7.96	8.36	8.84	9.45	10.26
0.4	7.03	7.25	7.49	7.78	8.11	8.51	8.99	9.60	10.41
0.5	7.21	7.42	7.67	7.95	8.29	8.68	9.17	9.79	10.60
0.6	7.42	7.64	7.88	8.17	8.50	8.90	9.39	10.01	10.83
0.7	7.70	7.92	8.16	8.45	8.79	9.19	9.68	10.30	11.12
0.8	8.08	8.30	8.55	8.84	9.17	9.58	10.07	10.69	11.51

As the height taper ratio and width taper ratio increase, first natural frequancy is also increase for non-rotating BBT beam. As you can see from table, height taper ratio and width taper ratio are almost same effective on first natural frequancy.

Table 13: 2.Natural Frequancy of Non-rotating BBT Euler Bernolli Beam

	c_b								
c_h	0	0.1	0.2	0.3	0.4	0.5	0.6	0.7	0.8
0	23.04	23.38	23.76	24.20	24.71	25.33	26.08	27.06	28.39
0.1	23.79	24.13	24.51	24.95	25.47	26.09	26.85	27.83	29.17
0.2	24.65	24.99	25.37	25.81	26.33	26.95	27.72	28.70	30.05
0.3	25.63	25.97	26.36	26.81	27.33	27.95	28.72	29.71	31.06
0.4	26.78	27.13	27.52	27.97	28.49	29.12	29.89	30.89	32.25
0.5	28.16	28.51	28.91	29.36	29.89	30.52	31.30	32.30	33.67
0.6	29.85	30.20	30.60	31.06	31.59	32.23	33.01	34.02	35.40
0.7	31.68	31.99	32.33	32.73	33.19	33.74	34.42	35.32	36.60
0.8	30.10	30.39	30.72	31.10	31.53	32.06	32.71	33.56	34.79

As the height taper ratio and width taper ratio increase, second natural frequancy is also increase for non-rotating BBT beam. As you can see from table, height taper ratio and width taper ratio are almost same effective on second natural frequancy.

Table 14: 3.Natural Frequancy of Non-rotating BBT Euler Bernolli Beam

	c_b								
c_h	0	0.1	0.2	0.3	0.4	0.5	0.6	0.7	0.8
0	41.08	41.48	41.94	42.45	43.05	43.77	44.65	45.80	47.41
0.1	39.88	40.27	40.71	41.21	41.79	42.49	43.34	44.46	46.02
0.2	38.64	39.02	39.45	39.93	40.49	41.17	41.99	43.07	44.60
0.3	37.36	37.73	38.14	38.61	39.15	39.80	40.60	41.64	43.12
0.4	36.03	36.38	36.78	37.23	37.75	38.38	39.15	40.16	41.59
0.5	34.64	34.98	35.36	35.79	36.30	36.90	37.64	38.62	40.00
0.6	33.19	33.52	33.88	34.29	34.78	35.35	36.07	37.00	38.33
0.7	31.97	32.33	32.74	33.20	33.75	34.39	35.18	36.20	37.58
0.8	34.76	35.13	35.55	36.03	36.58	37.24	38.04	39.07	40.45

While the height taper ratio is increasing, third natural frequancy is decreasing for non-rotating BBT beam. As width taper ratio increase natural frequancy increase also. As you can see from table, taper ratios have different effect on third natural frequancy.

Table 15: 4.Natural Frequancy of Non-rotating BBT Euler Bernolli Beam

	c_b								
c_h	0	0.1	0.2	0.3	0.4	0.5	0.6	0.7	0.8
0	114.88	115.26	115.70	116.20	116.80	117.54	116.31	111.0	105.6
0.1	110.11	110.49	110.92	111.42	112.00	112.72	113.65	112.1	106.6
0.2	105.21	105.59	106.01	106.49	107.07	107.77	108.66	109.8	107.8
0.3	100.16	100.52	100.94	101.41	101.97	102.65	103.52	104.7	106.4
0.4	94.92	95.28	95.68	96.14	96.69	97.35	98.19	99.32	101.0
0.5	89.46	89.80	90.20	90.64	91.17	91.81	92.62	93.70	95.32
0.6	83.71	84.05	84.43	84.86	85.37	85.99	86.76	87.80	89.33
0.7	77.60	77.93	78.29	78.71	79.20	79.79	80.52	81.51	82.96
0.8	70.99	71.30	71.65	72.05	72.51	73.06	73.76	74.68	76.04

While the height taper ratio and width taper ratio is increasing, fourth natural frequancy is decreasing for non-rotating BBT beam. As you can see from table height taper ratio is more effective on fourth natural frequancy.

Table 16: 1.Natural Frequancy of Rotating BBT Euler Bernolli Beam (50 rad/sn)

	c_b								
c_h	0	0.1	0.2	0.3	0.4	0.5	0.6	0.7	0.8
0	10.88	11.07	11.28	11.52	11.80	12.14	12.55	13.09	13.80
0.1	11.12	11.31	11.52	11.76	12.05	12.39	12.81	13.34	14.06
0.2	11.40	11.59	11.80	12.04	12.33	12.67	13.09	13.63	14.36
0.3	11.72	11.91	12.12	12.37	12.66	13.00	13.43	13.97	14.70
0.4	12.10	12.29	12.50	12.75	13.04	13.39	13.82	14.36	15.10
0.5	12.55	12.74	12.96	13.21	13.51	13.86	14.29	14.84	15.58
0.6	13.11	13.31	13.53	13.78	14.08	14.43	14.87	15.42	16.16
0.7	13.82	14.02	14.25	14.51	14.81	15.17	15.60	16.16	16.91
0.8	14.77	14.98	15.21	15.47	15.78	16.14	16.58	17.14	17.89

As the height taper ratio and width taper ratio increase, first natural frequancy is also increase for rotating BBT beam. As you can see from table, both taper ratios are same effective on first natural frequancy.

Table 17: 2.Natural Frequancy of Rotating BBT Euler Bernolli Beam(50 rad/sn)

	c_b								
c_h	0	0.1	0.2	0.3	0.4	0.5	0.6	0.7	0.8
0	24.87	25.63	26.49	27.49	28.66	30.06	31.78	33.95	36.80
0.1	25.25	26.01	26.87	27.87	29.05	30.45	32.17	34.35	37.22
0.2	25.67	26.43	27.30	28.30	29.48	30.89	32.62	34.80	37.68
0.3	26.16	26.92	27.79	28.80	29.98	31.40	33.13	35.32	38.21
0.4	26.73	27.50	28.37	29.38	30.57	31.99	33.73	35.93	38.70
0.5	27.42	28.19	29.07	30.08	31.27	32.69	34.44	36.65	39.23
0.6	28.27	29.04	29.92	30.94	32.13	33.56	35.31	37.53	39.89
0.7	29.35	30.13	31.02	32.04	33.24	34.68	36.44	38.66	40.76
0.8	30.84	31.62	32.52	33.55	34.76	36.20	37.97	40.20	42.04

When the height taper ratio and width taper ratio is increasing of beam, second natural frequancy is also increasing for rotating BBT beam. As you can see from table width taper ratio is more effective on second natural frequancy.

Table 18: 3.Natural Frequancy of Rotating BBT Euler Bernolli Beam(50 rad/sn)

	c_b								
c_h	0	0.1	0.2	0.3	0.4	0.5	0.6	0.7	0.8
0	46.21	45.16	44.08	42.98	41.85	40.70	39.54	38.38	37.28
0.1	46.61	45.54	44.45	43.34	42.20	41.04	39.86	38.69	37.57
0.2	47.06	45.98	44.87	43.74	42.59	41.41	40.22	39.03	37.89
0.3	47.58	46.48	45.36	44.21	43.04	41.84	40.63	39.42	38.27
0.4	48.17	47.06	45.92	44.75	43.56	42.34	41.11	39.88	38.83
0.5	48.89	47.75	46.59	45.40	44.19	42.95	41.69	40.43	39.56
0.6	49.78	48.61	47.42	46.21	44.97	43.70	42.41	41.12	40.46
0.7	50.94	49.75	48.52	47.27	45.99	44.69	43.36	42.04	41.60
0.8	52.60	51.36	50.09	48.79	47.47	46.11	44.74	43.36	43.14

As the height taper ratio increase of beam, third natural frequancy is decreasing for rotating BBT beam while width taper ratio increasing fourth natural frequancy is also increasing As you can see from table, taper ratios have different effect on third natural frequancy.

Table 19: 4.Natural Frequancy of Rotating BBT Euler Bernolli Beam (50 rad/sn)

	c_b								
c_h	0	0.1	0.2	0.3	0.4	0.5	0.6	0.7	0.8
0	120.88	116.25	111.50	106.61	101.56	96.34	90.88	85.14	79.04
0.1	121.28	116.64	111.87	106.98	101.92	96.69	91.22	85.47	79.34
0.2	121.73	117.07	112.30	107.39	102.33	97.08	91.60	85.84	79.69
0.3	122.24	117.58	112.79	107.87	102.80	97.53	92.04	86.25	80.09
0.4	122.86	118.18	113.38	108.44	103.35	98.07	92.55	86.74	80.55
0.5	123.61	118.91	114.09	109.13	104.02	98.71	93.17	87.33	81.11
0.6	119.47	119.84	115.00	110.01	104.87	99.53	93.95	88.08	81.81
0.7	114.32	115.40	116.23	111.21	106.02	100.63	95.00	89.07	82.74
0.8	108.99	110.01	111.17	112.49	107.73	102.27	96.56	90.54	84.12

As the height taper ratio increase of beam, fourth natural frequancy is decreasing for rotating BBT beam while width taper ratio increasing fourth natural frequancy is also increasing till critical taper ratio. As you can see from table width taper ratio is more effective on fourth natural frequancy.

In below figures, the first fourth natural frequencies of a rotating tapered Euler-Bernoulli beam with respect to the rotational speed parameter, Ω and the variation of taper ratios, Cb and Ch, is shown. In addition, first four figures shows that effect on natural frequencies when Cb is constant and Ch is variable. The other four figures shows that effect on natural frequencies when Ch is constant and Cb is variable.

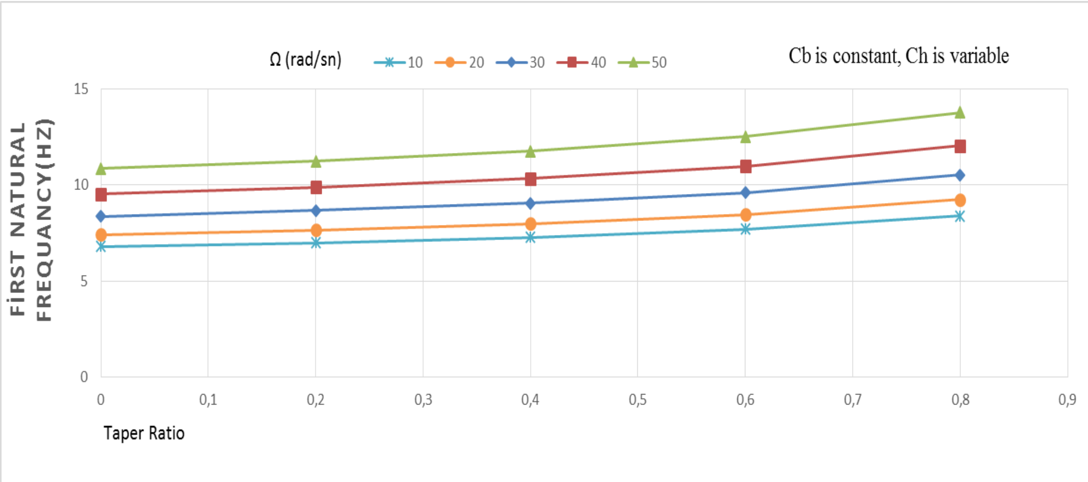

Figure 17: Variation of the first natural frequency with respect to Cb is constant, Ch is variable and the rotational speed parameter **Ω**.

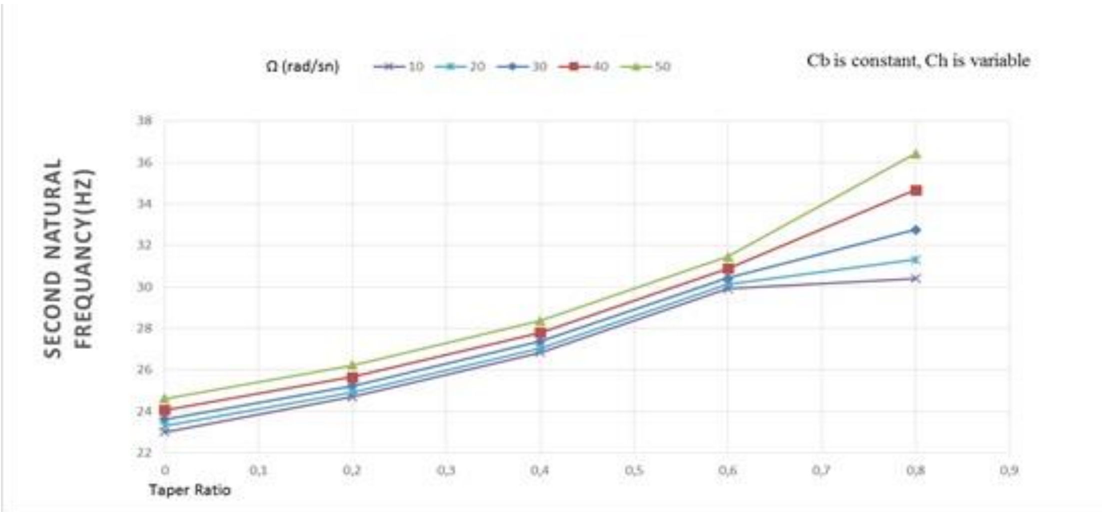

Figure 18: Variation of the second natural frequency with respect to Cb is constant, Ch is variable and the rotational speed parameter **Ω**.

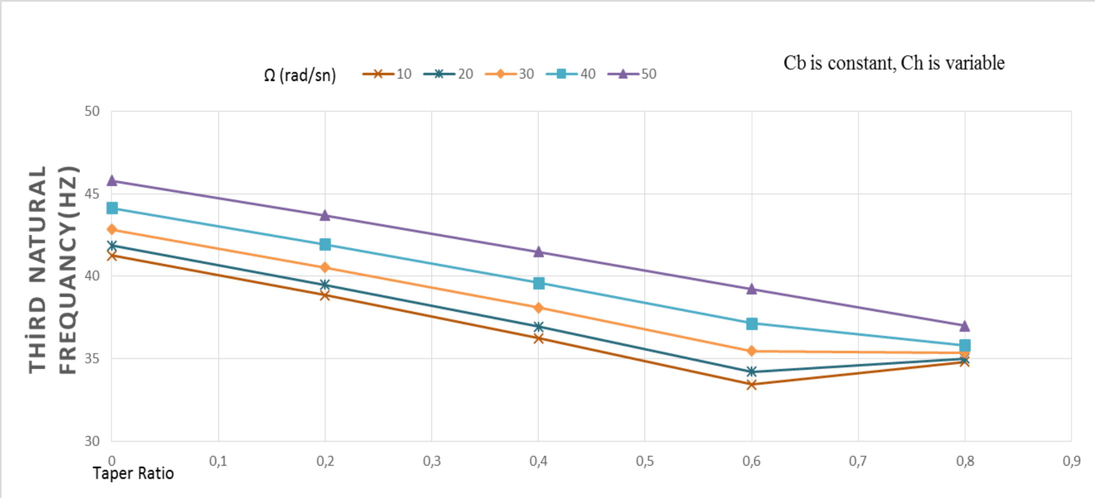

Figure 19: Variation of the third natural frequency with respect to Cb is constant, Ch is variable and the rotational speed parameter Ω.

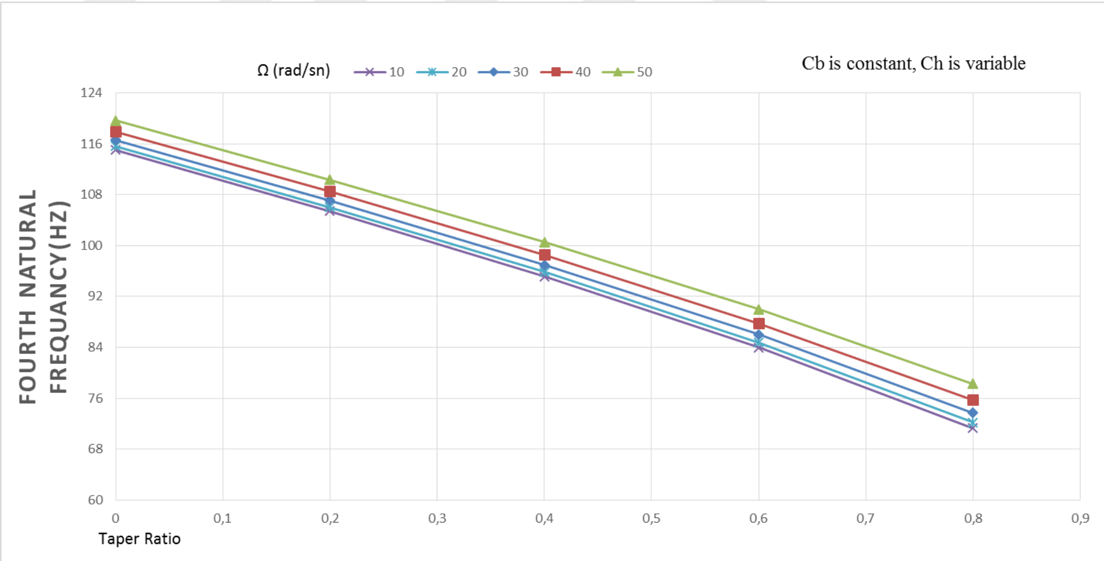

Figure 20: Variation of the fourth natural frequency with respect to Cb is constant, Ch is variable and the rotational speed parameter Ω.

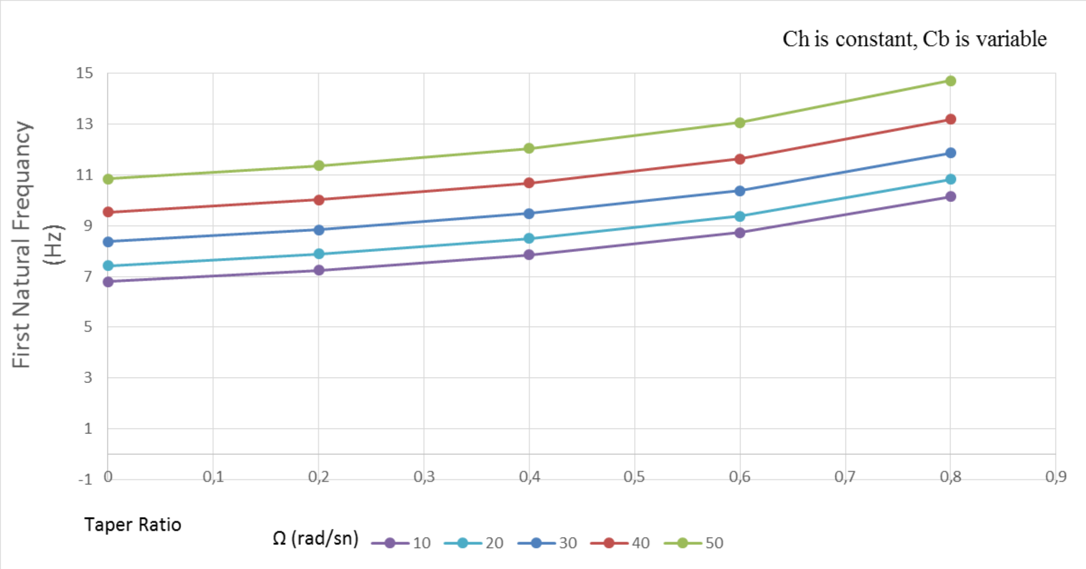

Figure 21: Variation of the first natural frequency with respect to Ch is constant, Cb is variable and the rotational speed parameter **Ω**.

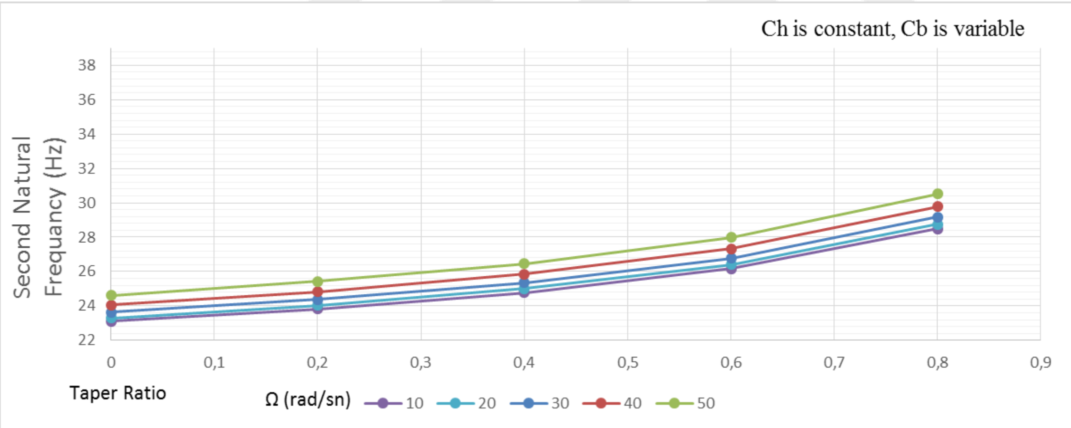

Figure 22: Variation of the second natural frequency with respect to Ch is constant, Cb is variable and the rotational speed parameter **Ω**.

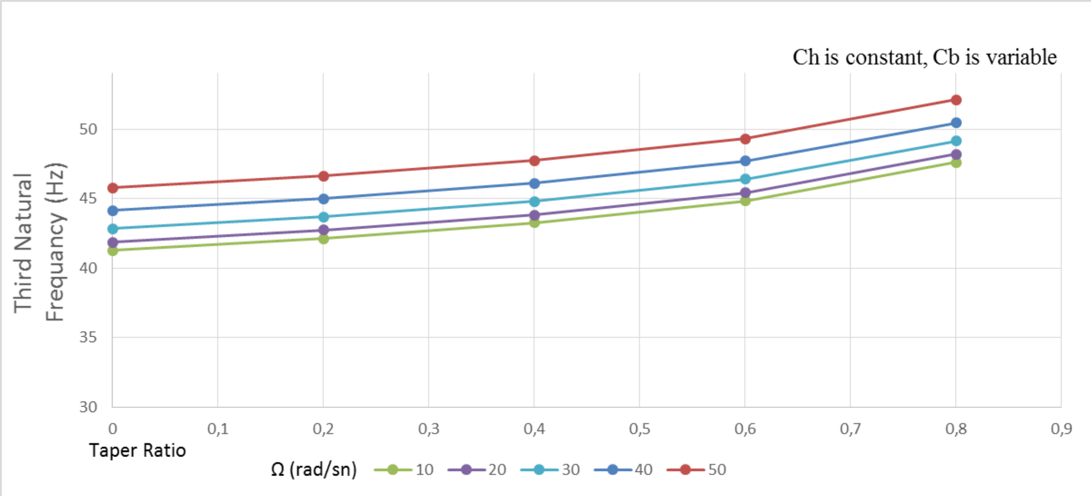

Figure 23: Variation of the third natural frequency with respect to Ch is constant, Cb is variable and the rotational speed parameter Ω.

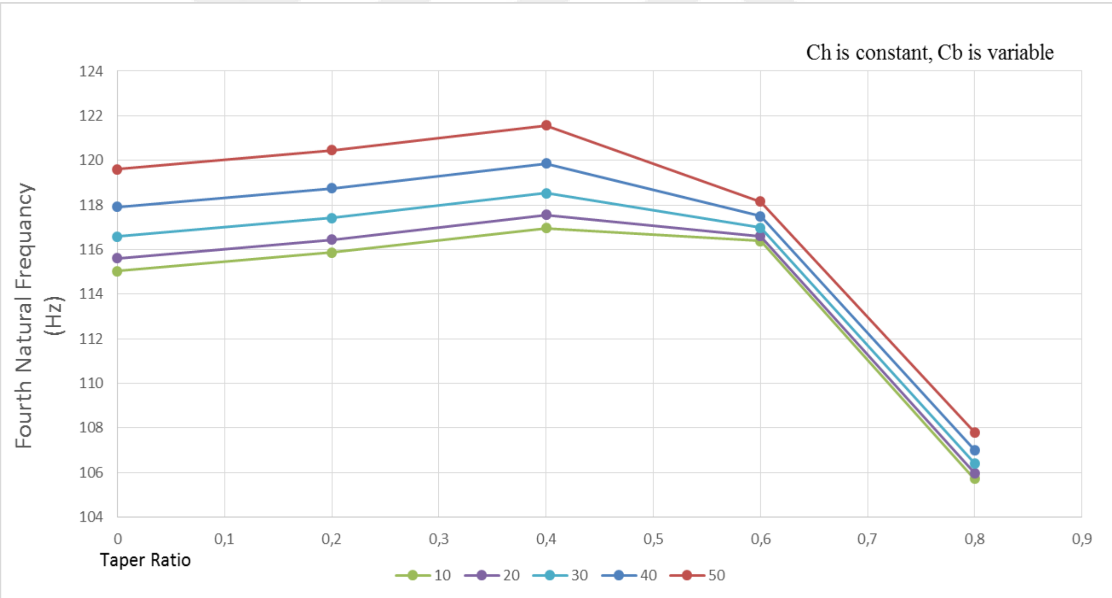

Figure 24: Variation of the fourth natural frequency with respect to Ch is constant, Cb is variable the and rotational speed parameter Ω.

It is noticed that rotational speed has an increasing affect on the natural frequencies because of the increasing centrifugal force that makes the beam stiffer. Centrifugal force is directly commeasurable to the square of the rotational speed.

6. CONCLUSIONS AND RECOMMENDATIONS

This thesis study provides a simple procedure for obtaining stiffness and mass matrices. Tapered Euler's Bernoulli rectangular beam recommended procedure has been verified by pre-produced results and method. Shape functions, mass and The stiffness matrices are calculated for the beam using the Finite Element Method. It requires less computational effort due to the availability of the computer program.

The affects of taper ratios and the rotational speed on the natural frequencies are investigated. The following results are presented:

- It was seen that coupling is not much effect on basic frequency. YY bending mode frequancy is a little increasing when beam is coupled.
- At natural frequencies, the effect of rotation speed is more dominant than the taper ratio.
- The width taper ratio has an increasing effect on the natural frequencies of both bending and torsion.
- Mode shapes are drawn for different taper ratios.
- The height taper ratio has a increasing effect on the fundamental first two natural frequency. Third and fourth natural frequencies decrease as the height taper ratio increases.
- The torsional frequencies decrease as height ratio increase while its increase up to value called the critical taper ratio then decrease as width taper ratio increase.

Future studies in this direction will aim to implement the applying to above methods for pre-twist and functionally graded tapered beams show results. The Bernoulli beam gives a more practical idea about the beamvibration frequency and mode shapes.Timoshenko beam will be use for how to effect of shear to free vibration and element number can be increase. Mass can be put end of the taper beam and mode analysis can be performed.

REFERENCES

[1] **Özdemir, Ö., & Kaya, M. O.** (2006). Flapwise bending vibration analysis of a rotating tapered cantilever Bernoulli–Euler beam by differential transform method. *Journal of Sound and Vibration*, *289*(1-2), 413-420.

[2] **Ozgumus, O. O., & Kaya, M. O.** (2008). Flapwise bending vibration analysis of a rotating double-tapered Timoshenko beam. *Archive of Applied Mechanics*, *78*(5), 379-392.

[3] **Mabie, H. H., & Rogers, C. B.** (1968). Transverse vibrations of tapered cantilever beams with end support. *The Journal of the Acoustical Society of America*, *44*(6), 1739-1741.

[4] **Ece, M. C., Aydogdu, M., & Taskin, V.** (2007). Vibration of a variable cross-section beam. *Mechanics Research Communications*, *34*(1), 78-84.

[5] **Bazoune, A., & Khulief, Y. A.** (1992). A finite beam element for vibration analysis of rotating tapered Timoshenko beams. *Journal of Sound and Vibration*, *156*(1), 141-164.

[6] **Banerjee, J. R., & Williams, F. W**. (1985). Exact Bernoulli–Euler dynamic stiffness matrix for a range of tapered beams. *International Journal for Numerical Methods in Engineering*, *21*(12), 2289-2302.

[7] **Raju, K. K., Shastry, B. P., & Rao, G. V.** (1976). A finite element formulation for the large amplitude vibrations of tapered beams. *Journal of Sound Vibration*, *47*, 595-598.

[8] **Mabie, H. H., & Rogers, C. B.** (1974). Transverse vibrations of double-tapered cantilever beams with end support and with end mass. *The Journal of the Acoustical Society of America*, *55*(5), 986-991.

[9] **Gupta, R. S., & Rao, S. S.** (1978). Finite element eigenvalue analysis of tapered and twisted Timoshenko beams. *Journal of Sound and vibration*, *56*(2), 187-200.

[10] **Hodges, D. H.** (1976). Stability of elastic bending and torsion of uniform cantilever rotor blades in hover with variable structural coupling.

[11] **Ozgumus, O. O., & Kaya, M. O**. (2007). Energy expressions and free vibration analysis of a rotating double tapered Timoshenko beam featuring bending–torsion coupling. *International journal of engineering science*, *45*(2-8), 562-586.

[12] **To, C. W. S.** (1981). A linearly tapered beam finite element incorporating shear deformation and rotary inertia for vibration analysis. *Journal of Sound and Vibration*, *78*(4), 475-484.

[13] **Özdemir, Ö.** (2012). *ADYNAMIC AND AEROELASTIC ANALYSIS OF A HELICOPTER BLADE WITH AN ACTIVELY CONTROLLED TRAILING EDGE FLAP IN FORWARD FLIGHT*. (Doktora tezi). ISTANBUL Teknik Üniversitesi, Fen Bilimleri Enstitüsü, ISTANBUL.

CURRICULUM VITAE

Name Surname : **Yunus Emre COŞKUN**

Place and Date of Birth : **Kırşehir 10.06.1991**

E-Mail : **yunusemrecoskun2@gmail.com**

EDUCATION :

- **B.Sc.** : 2015, Istanbul Technical University, Aeronautical and Astronautical Faculty, Aeronautical Engineering
- **M.Sc.** : 2019, Istanbul Technical University, Aeronautical and Astronautical Faculty, Aeronautical and Astronautical Engineering

PROFESSIONAL EXPERIENCE AND REWARDS:

- 2015-2016 Research Engineer in ISTANBUL Technical University at DKTM.
- 2017-2018 Research Engineer in ISTANBUL Technical University at DKTM
- 2018-Turkish Aerospace Indusrty Structural Design Engineer

PUBLICATIONS, PRESENTATIONS AND PATENTS ON THE THESIS:

- **Coşkun, Y.E., Özdemir, Ö.** 2016. 'Kompozit Bir Helikopter Palinin Katman Dizilimlerinin Pal TitreşimÖzellikleri Üzerindeki Etkisinin İncelemesi', *VI. ULUSAL HAVACILIK VE UZAY KONFERANSI* UHUK-2016-040